

**Plateau reduction by drainage divide migration in the Eastern Cordillera of Colombia defined by morphometry and <sup>10</sup>Be terrestrial cosmogenic nuclides**

Journal:	<i>Earth Surface Processes and Landforms</i>
Manuscript ID	ESP-15-0410.R2
Wiley - Manuscript type:	Paper
Date Submitted by the Author:	n/a
Complete List of Authors:	Struth, Lucía; Universitat Autònoma de Barcelona, Departament de Geologia Teixell, Antonio ; Universitat Autònoma de Barcelona, Departament de Geologia Owen, Lewis; University of Cincinnati, Geology Babault, Julien; Universitat Autònoma de Barcelona, Departament de Geologia
Keywords:	Cosmogenic nuclides, Drainage evolution, Divide migration, Eastern Cordillera of Colombia, Erosion rates

SCHOLARONE™  
Manuscripts

Post-print of: Struth, Lucía et al. "Plateau reduction by drainage divide migration in the Eastern Cordillera of Colombia defined by morphometry and Be terrestrial cosmogenic nuclides" in *Earth Surface Processes and Landforms* (2016). The final version is available at DOI 10.1002/esp.4079

1  
2  
3  
4  
5 1 **Plateau reduction by drainage divide migration in the Eastern**  
6  
7  
8 2 **Cordillera of Colombia defined by morphometry and  $^{10}\text{Be}$**   
9  
10 3 **terrestrial cosmogenic nuclides**  
11  
12  
13 4  
14

15 5 Lucía Struth<sup>1‡</sup>, Antonio Teixell<sup>1</sup>, Lewis A. Owen<sup>2</sup>, Julien Babault<sup>1</sup>  
16  
17  
18 6

19  
20  
21 7 <sup>1</sup> Departament de Geologia, Universitat Autònoma de Barcelona, 08193 Bellaterra,  
22  
23 8 Barcelona, Spain

24  
25  
26 9 <sup>2</sup> Department of Geology, University of Cincinnati, Cincinnati, OH 45221, USA  
27  
28

29 10 +34935811035/+34935811263, Lucia.Struth@gmail.com  
30  
31

32 11 <sup>‡</sup> Corresponding author  
33  
34  
35

36 12 **ABSTRACT**  
37

38 13 Catchment-wide erosion rates were defined using  $^{10}\text{Be}$  terrestrial cosmogenic nuclides  
39  
40 14 for the Eastern Cordillera of the Colombian Andes to help determine the nature of  
41  
42 15 drainage development and landscape evolution. The Eastern Cordillera, characterized  
43  
44 16 by a smooth axial plateau bordered by steep flanks, has a mean erosion rate of  $11 \pm 1$   
45  
46 17 mm/ka across the plateau and  $70 \pm 10$  mm/ka on its flanks, with local high rates of >  
47  
48 18 400 mm/ka. The erosional contrast between the plateau and its flanks was produced by  
49  
50 19 the increase in the orogen regional slope, derived from the progressive shortening and  
51  
52 20 thickening of the Eastern Cordillera. The erosion rates together with digital topographic  
53  
54 21 analysis show that the drainage network is dynamic and confirms the view that  
55  
56 22 drainage divides in the Eastern Cordillera are migrating towards the interior of the  
57  
58  
59  
60

1  
2  
3 23 mountain belt resulting in progressive drainage reorganization from longitudinal to  
4  
5 24 transverse-dominated rivers and areal reduction of the Sabana de Bogotá plateau.  
6  
7 25  
8

9 26 *Keywords:* Cosmogenic nuclides; Erosion rates; Drainage evolution; Divide migration;  
10  
11 27 Eastern Cordillera of Colombia.  
12  
13 28  
14  
15 29  
16

### 17 30 **1. Introduction**

18  
19 31 Rift inversion and/or crustal thickening result in dramatic topography and drainage  
20  
21 32 network changes in mountain belts that are mainly controlled by major tectonic  
22  
23 33 structures (e.g., Van der Beek et al., 2002). The evolution and development of drainage  
24  
25 34 systems in active orogens has attracted much attention recently, particularly with  
26  
27 35 regard to transverse and longitudinal drainages, and drainage divides (e.g., Willett et  
28  
29 36 al., 2001, 2014; Pelletier 2004; Bonnet et al., 2009; Castelltort et al., 2012; Perron et  
30  
31 37 al., 2012; Goren et al., 2014; Viaplana et al., 2015). Clear examples of drainage  
32  
33 38 rearrangement in relation to progressive mountain building have been described in the  
34  
35 39 inverted rifts of the High Atlas of Morocco (Babault et al., 2012) and Eastern Cordillera  
36  
37 40 of Colombia (Babault et al., 2013; Struth et al., 2015). These studies highlight that  
38  
39 41 drainage divides are dynamic features that progressively migrate and result in river  
40  
41 42 capture events. Providing evidence for differential erosion rates on either side of a  
42  
43 43 drainage divide adds much credence to developing and substantiating drainage  
44  
45 44 evolution models for mountain belts (e.g., Willett et al., 2014). As such, the side of a  
46  
47 45 mountain belt with the greatest erosion will progressively migrate and capture  
48  
49 46 drainages from the side with the least erosion. Theoretically, a dynamic drainage  
50  
51 47 network will evolve towards a steady state, maintaining a steady drainage network and  
52  
53 48 stationary drainage divides (Howard, 1965).  
54  
55  
56  
57  
58  
59  
60

1  
2  
3 49 The Eastern Cordillera of Colombia is an example of an orogen with a dynamic  
4  
5 50 drainage network (Babault et al., 2013; Struth et al., 2015). This N-S-oriented orogenic  
6  
7 51 belt has two topographic domains: i) an axial zone with low relief associated with  
8  
9 52 longitudinal rivers that have gentle gradients (the Sabana de Bogotá); and ii) high-relief  
10  
11 53 flanks with steeper transverse rivers. These domains are separated by what we refer to  
12  
13 54 as the eastern and western main drainage divides. Recent studies have suggested that  
14  
15 55 the increase of regional slopes due to progressive crustal thickening results in fluvial  
16  
17 56 reorganization from longitudinal to transverse dominated drainages in the Eastern  
18  
19 57 Cordillera (Babault et al., 2013; Struth et al., 2015). On the basis of a morphometric  
20  
21 58 analysis, field observations and a summary of paleodrainage data, these studies  
22  
23 59 conclude that drainage reorganization takes place by progressive drainage divide  
24  
25 60 migration toward the axial zone of the orogen by a step-by-step series of river captures.

26  
27  
28 61 In this study, we build on the work of Struth et al. (2015) by using  $^{10}\text{Be}$  terrestrial  
29  
30 62 cosmogenic nuclides (TCNs) in fluvial sands to determine catchment-wide erosion  
31  
32 63 rates for the Eastern Cordillera to investigate the contrasting erosion dynamics  
33  
34 64 between the Sabana de Bogotá axial plateau and the flanks of the Eastern Cordillera.  
35  
36 65 TCN analysis is combined with a comparative analysis of steepness index, specific  
37  
38 66 stream power and the integral of the drainage area ( $\chi$  values). We also examine the  
39  
40 67 role of local tectonics, lithology, and climate conditions as a control on drainage  
41  
42 68 evolution.

## 43 44 45 69 46 47 48 70 **2. Geological, morphological and climatological setting**

49  
50 71 The Eastern Cordillera of Colombia is an inverted continental rift in the northern  
51  
52 72 Andes. The cordillera is composed of Precambrian-Paleozoic basement and a  
53  
54 73 succession of Mesozoic and early Cenozoic sedimentary rocks within a doubly-verging  
55  
56 74 thrust system (Julivert, 1970; Colletta et al., 1990; Cooper et al., 1995; Fig. 1).

1  
2  
3 75 The Eastern Cordillera is flanked on both sides by lowlands composed of  
4  
5 76 Cenozoic deposits, which infill the Magdalena Valley and the Llanos foreland basins  
6  
7 77 that are at elevations of ~200-300 m above mean sea level (asl; Fig. 1A). The flanks of  
8  
9 78 the Eastern Cordillera are dominated by alternating Cretaceous sandstone and shale  
10  
11 79 formations. Isolated Precambrian-Paleozoic basement massifs with low- and medium-  
12  
13 80 grade metamorphic rocks (mainly phyllite and schist) are present in the Quetame and  
14  
15 81 Floresta massifs (Segovia, 1965; Ulloa and Rodríguez, 1979; Ulloa and Rodríguez,  
16  
17 82 1982; Parra et al., 2009a; Fig. 1A,B). The axial plateau of the Sabana de Bogotá is  
18  
19 83 dominated by Cretaceous to Paleogene sandstone and shale that are deformed into  
20  
21 84 open folds, whereas the Cordillera foothills have foreland facing thrust faults with large-  
22  
23 85 displacement (e.g., Mora et al., 2008 and references therein; Fig. 1B). The local  
24  
25 86 relief in the Sabana de Bogotá plateau is small because up to 600 m of unconformable  
26  
27 87 Pliocene-Quaternary fluviolacustrine deposits partially fill the synclinal depressions  
28  
29 88 (Tilatá and Sabana formations; Julivert, 1963; Andriessen et al., 1993; Torres et al.,  
30  
31 89 2005). A moderate amount of orogenic shortening, 25 to 30%, across the Eastern  
32  
33 90 Cordillera has been calculated along serial transects by Tesón et al. (2013) and Teixell  
34  
35 91 et al. (2015).

36  
37  
38 92 There is a strong precipitation gradient across the western divide, whereas no  
39  
40 93 precipitation gradient exists across the eastern divide (Fig. 2). Precipitation is greatest  
41  
42 94 (> 3000 mm/yr) near Charalá, in the eastern and western foothills and in the Quetame  
43  
44 95 Massif.

## 45 46 47 96 48 49 50 97 *2.2 Summary of the deformation and paleodrainage evolution of the Eastern Cordillera*

51  
52 98 Paleogene data show a western and southwestern source for the Central  
53  
54 99 Cordillera foreland basin sediments, which currently include the early successions of  
55  
56 100 deposits in the Magdalena Valley and Llanos basins, and the intervening Eastern  
57  
58  
59  
60

1  
2  
3 101 Cordillera. Sediments moved NNE in the Central Cordillera foreland basin following the  
4  
5 102 regional slope and the contemporaneous structures within the basin (e.g., Cooper et  
6  
7 103 al., 1995; Bayona et al., 2008; Silva et al., 2013). The drainage was longitudinal,  
8  
9 104 parallel to the current Eastern Cordillera, following growing folds that  
10  
11 105 thermochronological data show started to form during the Eocene (e.g., Parra et al.,  
12  
13 106 2009b; Mora et al., 2010; Moreno et al., 2011; Saylor et al., 2011; Caballero et al.,  
14  
15 107 2013a, 2013b; Silva et al., 2013).

16  
17 108 The Magdalena and the Llanos basins became disconnected by the uplift of the  
18  
19 109 Eastern Cordillera as deformation propagated eastward during the Late Oligocene to  
20  
21 110 Early Miocene (Parra et al., 2009b; Mora et al., 2010). This is supported by provenance  
22  
23 111 data indicating that the Eastern Cordillera developed into an effective topographic  
24  
25 112 barrier that separated the Central Cordillera from the Llanos basin before the Mid to  
26  
27 113 Late Miocene (Horton et al., 2010). The axial Eastern Cordillera was likely a closed  
28  
29 114 basin south of 6°N during the late Oligocene-Miocene (Silva et al., 2013).

30  
31 115 Base level started to rise in the Middle Magdalena Valley basin during the Late  
32  
33 116 Oligocene to Mid Miocene, forcing its rivers to flow to the east, across the present  
34  
35 117 location of the Eastern Cordillera, into the Llanos basin (Gómez et al., 2005b). The  
36  
37 118 drainage in the Middle Magdalena Valley basin returned to flow to the north due to the  
38  
39 119 continued uplift of the cordillera during the Mid-Late and Late Miocene. Since the Late  
40  
41 120 Miocene, the paleoflow pattern in the eastern foreland of the Eastern Cordillera is  
42  
43 121 characterized by a transverse drainage reflecting an eastward direction (Parra et al.,  
44  
45 122 2010) and providing sediments for the Llanos and Middle Magdalena Valley basins.  
46  
47 123 Most external thrust sheets of the Cordillera are strongly deformed in recent times, and  
48  
49 124 there are very young apatite fission track ages for the Quetame Massif along its  
50  
51 125 eastern flank (0-3 Ma; Fig. 3). This attests to strong exhumation across the Eastern  
52  
53 126 Cordillera margins in the latest Neogene and Quaternary (Mora et al., 2008) .  
54  
55  
56  
57  
58  
59  
60

1  
2  
3 127 Struth et al. (2015) argue that the Eastern Cordillera is experiencing fluvial  
4  
5 128 drainage network reorganization by drainage divide migration. Longitudinal drainages  
6  
7 129 created in the early stages of drainage developed paralleling the structural grain of the  
8  
9 130 growing tectonic orogen. The potential energy and power of transverse rivers was  
10  
11 131 enhanced as the regional slope progressively increased during crustal thickening. This  
12  
13 132 resulted in headward erosion causing drainage divide migration towards the Sabana  
14  
15 133 plateau and capturing longitudinal streams: ultimately leading to drainage network  
16  
17 134 reorganization.

18  
19  
20 135

### 21 136 **3. Methods**

#### 22 137 *3.1. Analysis of the digital drainage network*

23  
24  
25 138 We used digital elevation model (DEM) SRTM90v4 that has a horizontal  
26  
27 139 resolution of 90 m (Jarvis et al., 2008) to analyze the drainage network for the Eastern  
28  
29 140 Cordillera. The DEM was corrected in narrow areas that had low resolution using  
30  
31 141 elevations from Instituto Geográfico Agustín Codazzi (IGAC) 1:100,000 topographic  
32  
33 142 maps. Various geomorphic parameters provide information about erosion in channel  
34  
35 143 networks and therefore information about the dynamism of the drainage. The most  
36  
37 144 important parameters that we examine include stream power, steepness index and  $\chi$ .  
38  
39 145 We calculated these parameters to characterize the contrast between the topographic  
40  
41 146 domains of the Sabana de Bogotá plateau and its flanks, and to identify which one best  
42  
43 147 correlates with the TCN-derived erosion rates. We propose that a correlation between  
44  
45 148 geomorphic parameters and TCN-derived erosion rates may allow a first estimation of  
46  
47 149 erosion rates in areas devoid of TCN data.

48  
49  
50  
51  
52 150 Stream power relates to the energy rate per unit distance along a river (Bagnold,  
53  
54 151 1966) and reflects the incision power of a river into bedrock under detachment-limited  
55  
56 152 conditions (e.g., Howard and Kerby, 1983; Howard et al., 1994; Whipple and Tucker,  
57  
58  
59  
60

1  
2  
3 153 1999; Kirby and Whipple, 2001). River incision is calculated according to the stream  
4  
5 154 power model expressed as:

6  
7  
8 155 
$$\partial z_{(x,t)}/\partial t = U_{(x,t)} - (KA^m S^n)_{(x,t)} \quad (1)$$
  
9  
10

11 156 where (U) represents the bedrock uplift at x, (K) is the erosional efficiency, (A) is local  
12  
13 157 drainage area and (S) is the channel slope. The positive exponents m and n describe  
14  
15 158 the relative dependency of stream erosion rates on A and S.

16  
17  
18 159 Analysis of slope-area has been frequently used to reveal erosion trends in channel  
19  
20 160 networks defined as steepness index or Ksn (Kirby and Whipple, 2001; Kirby, 2003;  
21  
22 161 Snyder et al., 2003; Wobus et al., 2006; Dibiase et al., 2010). However, local slope  
23  
24 162 calculations undertaken for regions that have low DEM resolution such as the Eastern  
25  
26 163 Cordillera of Colombia provide scattered and noisy results. For this reason, we  
27  
28 164 calculate the channel slopes using the  $\chi$  gradient referred to as Mx (Perron and  
29  
30 165 Royden, 2013; Mudd et al., 2014). To calculate Mx, we use the river profile elevation  
31  
32 166 instead of the slope as the dependent variable, against  $\chi$  as the independent variable.  
33  
34 167 This approach produces more reliable results. We plot values of Mx, i.e., the slope in  
35  
36 168  $\chi$ -elevation space (Mudd et al., 2014), a parameter related to the ratio between erosion  
37  
38 169 rate and erodibility (Perron and Royden, 2013), as a proxy to identify the distribution  
39  
40 170 and magnitude of erosion. We defined the best concavity of the river profiles based on  
41  
42 171 AICc-collinearity tests and  $\chi$ -plots following the method of Mudd et al. (2014) to  
43  
44 172 calculate Mx values. The AICc is a statistical method that selects a model that  
45  
46 173 balances goodness of the fit against model complexity (Akaike Information Criterion,  
47  
48 174 AICc; Akaike, 1974; Hurvich and Tsai, 1989; Burnham and Anderson, 2002). We  
49  
50 175 extract the AICc-collinearity test and the  $\chi$  plots for each basin based on  
51  
52 176 through a range of concavity values for the main channel and tributaries to define the  
53  
54 177 best-fit concavity. The concavity with the minimum AICc value will be the best fitting  
55  
56 178 one using this method. The mean calculated concavity for all the basins is 0.45 (see  
57  
58  
59  
60



1  
2  
3 179 SD1). We compared the  $M_x$  values between different catchments by fixing the obtained  
4  
5 180 concavity. Stream power theory predicts that river profiles will have a linear  $\chi$ -plot and  
6  
7 181 a  $M_x$  proportional to the erosion rates, assuming, firstly a steady-state condition, where  
8  
9 182 rock uplift is balanced by erosion, and secondly, that erosion, erodibility and uplift are  
10  
11 183 constant through time and space (Royden and Perron, 2013; Mudd et al., 2014). In  
12  
13 184 reality,  $U$  and  $K$  can be variable in space and time, which are dependent upon the  
14  
15 185 tectonic and climatic history, and rock type. We calculated the concavity for all the  
16  
17 186 basins following the method of Mudd et al. (2014) by extracting the steepness index,  
18  
19 187 knickpoints and localize all the known active structures as well as highly erodible  
20  
21 188 lithologies to solve this problem. In the case of stepped channel profiles associated  
22  
23 189 with spatial or temporal changes in uplift rates, we used the colinearity test to identify  
24  
25 190 the best concavity for each catchment (Mudd et al., 2014). This technique allows the  
26  
27 191 magnitude and distribution of the erosion rates to be identified.

28  
29  
30 192 We extract the  $\chi$ -map following the method of Willett et al. (2014), and with a  
31  
32 193 same base level determined by the elevation of the most external tectonic structures  
33  
34 194 (300 m asl) and with a critical drainage area of  $1 \text{ km}^2$  to extract information about the  
35  
36 195 dynamics of the catchments. The main focus of this analysis rests on mapping  
37  
38 196 differences in  $\chi$ -coordinate values across drainage divides. Similar  $\chi$  values on both  
39  
40 197 sides of a drainage divide would suggest that the region is in equilibrium, while large  
41  
42 198 differences in  $\chi$  values across the drainage divide imply that river networks are in  
43  
44 199 disequilibrium where divide migration or river capture is likely to occur (Willett et al.,  
45  
46 200 2014). Drainage divides generally migrate towards the higher  $\chi$  values to achieve  
47  
48 200 equilibrium, and hence, catchments with high values are prone to capture and may  
49  
50 201 eventually disappear (Willett et al., 2014). We extract the  $\chi$ -map for the entire central  
51  
52 202 segment of the Eastern Cordillera as a proxy for the dynamics of the drainage divides  
53  
54 203 using a modified version of  $\chi$  that makes a correction factor for the precipitation (Yang  
55  
56 204 et al., 2015) such that the  $\chi$  value is defined by the following  
57  
58 205  
59  
60

$$\int_0^x \left( \frac{P_0 A_0}{A(s^F) P(s^F)} \right)^m dx' \quad (2)$$

where  $P_0$  and  $A_0$  are arbitrary scaling factors for the precipitation rate and drainage area, respectively,  $P$  is precipitation rate,  $A$  is the upstream drainage area and  $m$  and  $n$  are empirical and non-integer constants.

We also calculated an averaged specific stream power (SSP, eq 3, Knighton, 1999) for each catchment following the method described in Godard (2012) such that:

$$SSP = d g K_{sn} Q/W \quad (3)$$

where  $d$  is density,  $g$  is acceleration due to gravity,  $K_{sn}$  is the steepness index slope,  $Q$  is discharge and  $W$  is the channel width.

### 3.2. Terrestrial cosmogenic nuclides analysis

Sediment samples were collected for  $^{10}\text{Be}$  TCN analysis to investigate erosional contrasts between the Sabana plateau and its flanks, including the main streams and major tributaries in the Guayuriba and Turmequé (representing the eastern flank of the Cordillera), Bogotá (Sabana de Bogotá plateau) and upper Suárez catchments. We followed the sampling methods of Carretier et al. (2015) who collected fluvial sand from the subcatchments to minimize issues associated with local lithologic variations. Rivers in the eastern flank and plateau have their headwaters on the same drainage divide, which allows us to make direct comparison between them. We also analyzed four  $^{10}\text{Be}$  TCN samples in the lower Suárez and Chicamocha catchments (Fig. 3, Table 1) to examine the effect of a different vegetation cover, bedrock erodibility and climate. These four samples are not included in the comparative analysis between the plateau domain and the eastern flank.

Larger sampled catchment areas have higher likelihoods of including mixed fluvial signatures. In such cases, the erosion rate obtained may not be representative

1  
2  
3 231 of all the reaches of that river, which may have experienced a diverse reorganization  
4  
5 232 history.

6  
7  
8 233 Catchments including a relict flat area in their upper parts (Chicamocha, Suárez,  
9  
10 234 Bogotá and Turmequé) reflect two different erosion regimes separated by a knickpoint  
11  
12 235 (white stars in Fig. 6). As such the upper part the catchment, above the mean  
13  
14 236 knickpoints, should have lower erosion rates (related to lower relief, gentler slopes and  
15  
16 237 lower Mx values) compared to those downstream. The Turmequé catchment illustrates  
17  
18 238 this well, with an ancient plateau domain above the main knickpoint where the erosion  
19  
20 239 rates are low (LUCN-45, 26) and higher erosion rates in its lower reaches (LUCN-25,  
21  
22 240 27, 28). We only sampled the upper part of the Bogotá catchment (LUCN-15, 19, 30,  
23  
24 241 31, 33) above the Tequendama Falls (see Fig.4 for location) to define the amount of  
25  
26 242 erosion in it lowest erosion rate domain. We sampled its gently sloping upper reaches  
27  
28 243 (LUCN-46, 50), and the steeper lower reaches below the knickpoint (LUCN-53, 55) in  
29  
30 244 the Suárez catchment. Only one sample (LUCN-53) was collected in the Chicamocha  
31  
32 245 valley catchment, which was located downstream of the main knickpoint.

33  
34  
35 246 We collected ~1 kg of sand for each sample. Catchment areas for each sample  
36  
37 247 were large (>100 km<sup>2</sup>) as recommended by Niemi et al. (2005) and Yanites et al.  
38  
39 248 (2005) to provide a good representation of the <sup>10</sup>Be TCN inventory and the erosion  
40  
41 249 rates. We use the erosion values obtained in the upstream reaches of the rivers that  
42  
43 250 flank the Eastern Cordillera to compare the erosion rates between the rivers of the  
44  
45 251 Sabana and the flanks of the cordillera. These flank rivers and the located in the  
46  
47 252 Sabana, flow through alternating sandstone and shale formations in proportions that  
48  
49 253 are similar in each different catchment. This similarity reduces the possibility of  
50  
51 254 lithological biasing in sampling between our chosen catchments. The erosion rates  
52  
53 255 determined by <sup>10</sup>Be reflect erosion on timescales of tens of thousands of years  
54  
55 256 (Blanckenburg, 2006). Additionally, we sampled rivers across the western flank of the  
56  
57 257 Eastern Cordillera, but we could not determine <sup>10</sup>Be concentrations in this region  
58  
59  
60

1  
2  
3 258 because we were unable to extract quartz from samples which were dominated by  
4  
5 259 argillaceous sediment.  
6  
7

8 260 We also collected five quartzite samples for  $^{10}\text{Be}$  TCN surface exposure dating  
9  
10 261 from a well-preserved river terrace in the Guayuriba Basin (Fig. 3C, Table 2). Such  
11  
12 262 landforms are rare in our study area. Our sampled river terrace, which lies at ~406 m  
13  
14 263 above the current stream, is not deformed, and it shows no evidence of erosion or  
15  
16 264 landsliding. We collected ~500 g rock from the upper surfaces of fresh quartzite  
17  
18 265 boulders inset into the river terrace. Topographic shielding was calculated by  
19  
20 266 measuring the inclination to the skyline for every cardinal and intercardinal direction  
21  
22 267 following the approach by Balco and Stone (2007).  
23  
24

25 268 Quartz isolation, purification, dissolution and preparation of BeO were undertaken  
26  
27 269 in the geochronology laboratories at the University of Cincinnati following the methods  
28  
29 270 of Kohl and Nishiizumi (1992) and described in detail in Dortch et al. (2009). All river  
30  
31 271 sediment and river terrace boulder samples were sieved and crushed to 250-500  $\mu\text{m}$   
32  
33 272 for the analysis. Samples were cleaned using  $\text{HNO}_3$ ,  $\text{HCl}$  and  $\text{HF}$  and passed through a  
34  
35 273 Frantz magnetic separator. Density separation was undertaken using lithium  
36  
37 274 heteropolytungstate followed by an additional  $\text{HF}$  leach (Brown et al., 1991; Kohl and  
38  
39 275 Nishiizumi, 1992; Cerling and Craig, 1994). For each sample, 15-30 g of clean quartz  
40  
41 276 grains was dissolved in  $\text{HF}$  and  $\text{HNO}_3$  with 350 mg of  $^9\text{Be}$  carrier. Beryllium was  
42  
43 277 separated using anion and cation exchange columns Beryllium hydroxide was obtained  
44  
45 278 after fuming with  $\text{HClO}_4$  acid and passing through anion and cation exchange columns  
46  
47 279 (Bourlès, 1988; Brown et al., 1992). The  $\text{Be}(\text{OH})_2$  was heated in an oven at 750  $^\circ\text{C}$  to  
48  
49 280 form BeO and then loaded in steel target mixed with of Niobium (Nb) powder.  $^{10}\text{Be}/^9\text{Be}$   
50  
51 281 ratios were measured by Accelerator Mass Spectrometry in the Purdue Rare Isotope  
52  
53 282 Measurement (PRIME) Laboratory at Purdue University, Indiana, USA.  
54  
55  
56  
57  
58  
59  
60

1  
2  
3 283 We took the standard approach and assumed that the amount of  $^9\text{Be}$  in the  
4  
5 284 prepared quartz was negligible. Sometimes this may not be the case, and quartz may  
6  
7 285 contain some  $^9\text{Be}$ . Such cases are rare, and almost invariably occur when quartz is  
8  
9 286 derived from beryl-bearing granites or pegmatites, so that traces of Be and/or small  
10  
11 287 amounts of beryl exist in the supposedly pure quartz sample, as documented in some  
12  
13 288 areas of the Himalaya (Portenga et al., 2015). However, pegmatites and beryl-bearing  
14  
15 289 granites are not present in our study area. Any significant native  $^9\text{Be}$  is therefore highly  
16  
17 290 unlikely in our sampled quartz. If native  $^9\text{Be}$  is present then denudation rates calculated  
18  
19 291 from  $^{10}\text{Be}$  concentrations will be overestimates, and the calculated erosion rates should  
20  
21 292 be considered as apparent; however these rates can still be used for comparisons of  
22  
23 293 variation across a region of similar lithologies (Corbett et al., 2013; Portenga et al.,  
24  
25 294 2015).

26  
27  
28 295 To model catchment-wide erosion rates from  $^{10}\text{Be}$  results we assumed that: i)  
29  
30 296 the sediment volume is proportional to the erosion rate, i.e., the catchment is close to  
31  
32 297 steady-state; ii) all the sediment collected at the sample locality was well mixed; iii) the  
33  
34 298 contribution of quartz was homogeneous in the catchment; iv) that there is an isotopic  
35  
36 299 equilibrium within the catchment, i.e., TCNs production in the catchment equals the  
37  
38 300 transport of TCNs out of the catchment; and v) the erosional timescale was significantly  
39  
40 301 larger than the sediment transfer through the catchment (e.g., Lal and Arnold, 1985;  
41  
42 302 Granger et al., 1966; von Blanckenburg, 2005).

43  
44  
45 303 The corrected catchment-averaged production rates for  $^{10}\text{Be}$  were calculated for  
46  
47 304 each catchment using the SRTM90 digital elevation model following the method of  
48  
49 305 Dortch et al. (2011) using MATLAB v. 2008 and the scaling factors provided in Lal  
50  
51 306 (1990) and Stone (2000). With this method, the production rate for each pixel is  
52  
53 307 calculated accounting for shielding to make an average for all the pixels in the  
54  
55 308 catchment to obtain a spatially average production rate for the entire catchment (Lal,  
56  
57 309 1991). We use a  $^{10}\text{Be}$  half-life of  $1.36 \pm 0.07$  Ma (Nishiizumi et al., 2007), the scaling  
58  
59  
60

1  
2  
3 310 model of Lal (1990) and Stone (2000) and a sea-level high-latitude production rate of  
4  
5 311  $4.49 \pm 0.39$   $^{10}\text{Be}$  atoms/g  $\text{SiO}_2/\text{a}$ , for catchment erosion rates and river terrace dating.  
6  
7  
8 312  $^{10}\text{Be}$  ages for the river terrace samples were calculated using the CRONUS  
9  
10 313 calculator (<http://hess.ess.washington.edu/math/>; Balco et al., 2008). These ages will  
11  
12 314 be minimum values and hence the resulting incision rates are maximum values. We  
13  
14 315 are aware that the production rates and scaling models for  $^{10}\text{Be}$  are being refined  
15  
16 316 (Borchers et al., 2016; Marrero et al., 2016). Borchers et al. (2016) recently revised the  
17  
18 317 production rate for sea level at high latitudes to  $4.01$   $^{10}\text{Be}$  atom/g  $\text{SiO}_2/\text{a}$  for Lal  
19  
20 318 (1990)/Stone (2000) scaling model. However, we prefer to use the established scaling  
21  
22 319 model and production rates in Balco et al. (2008) until there is community-wide  
23  
24 320 agreement on the appropriate production and scaling. The new production rate results  
25  
26 321 in an  $\sim 10\%$  difference in the erosion rate from our preferred values.

## 322 **4. Results**

### 323 *4.1. Digital drainage analysis*

324 The axial zone, which includes the Sabana de Bogotá and the southern part of  
325 the Sogamoso basin, is characterized by the lowest SSP values (Fig. 4). In contrast,  
326 higher SSP values occur on the Eastern Cordillera flanks and in the northern areas of  
327 the Sogamoso basin, which argue for higher erosion rates than in the axial zone of the  
328 cordillera.

329 We extend the  $M_x$  map for the Eastern Cordillera of Colombia of Struth et al.  
330 (2015) that was limited to the area between  $4^\circ\text{N}$  and  $5^\circ 30'\text{N}$  to between  $4^\circ\text{N}$  and  $7^\circ\text{N}$ .  
331 The  $M_x$  values have a similar distribution to the SSP, with higher values on the flanks  
332 and in the northern part of the Sogamoso basin than in the axial zone. The incision  
333 capacity is low (with low SSP) and values of  $M_x$  are also generally low ( $M_x=0-3$ ) in the  
334 Sabana plateau and the southern part of the Sogamoso basin. The eastern flank has  
335 average  $M_x$  values of between 5 and 12, with peak values between 20 and 27. Areas

1  
2  
3 336 of recent tectonic uplift such as the Farallones and Santa Maria anticlines (Mora et al.,  
4  
5 337 2008), or where rivers dramatically increase gradient when they exit the high-elevation  
6  
7 338 plains such as at the Tequendama Falls or at Chingaza, have the highest Mx values.  
8  
9 339 The upper Sogamoso basin, with northward drainage, has low Mx values and is similar  
10  
11 340 to those for Sabana de Bogotá. The Suárez basin has values between 4 and 7, while  
12  
13 341 the Chicamocha basin has values between 6 and 12. Local high Mx values are  
14  
15 342 associated with deeply incised stretches of the Suárez and Chicamocha rivers. Mx  
16  
17 343 values in the higher parts of the western flank, bordering the divide, where rivers are of  
18  
19 344 transverse type, range from ~5 to 12; Mx values decrease to between 1 and 4 in the  
20  
21 345 lower part of the flank where the rivers are of longitudinal type. River profiles in  $\chi$  space  
22  
23 346 are shown in the Supplementary Data (SD2) and were partly published in Struth et al.  
24  
25 347 (2015).

26  
27  
28 348 The  $\chi$  values in the axial region of Sabana de Bogotá of the Eastern Cordillera  
29  
30 349 (Fig. 5) are higher than those for its flanks in the area of the drainage divide. A strong  
31  
32 350 differentiation in  $\chi$  values exists within the same domain: while the Sabana de Bogotá  
33  
34 351 has low values near the central divide, the Sogamoso basin shows high values near  
35  
36 352 the divide (Fig. 5B1). In addition,  $\chi$  values indicate disequilibrium between the  
37  
38 353 Turmequé (with low values) and the Chicamocha (with higher values near the divide)  
39  
40 354 basins (Fig. 5B2).

41  
42  
43  
44 355 Low SSP, Mx and precipitation, and high  $\chi$  values in the headwaters of the rivers  
45  
46 356 characterize the plateau, while high SSP, Mx and precipitation, and low  $\chi$  values in the  
47  
48 357 headwaters of the rivers characterize the flanks. In summary, the geomorphic indices  
49  
50 358 clearly differentiate the plateau and flank domains within the Eastern Cordillera.  
51  
52 359

## 360 4.2. Landscape evolution rates

361 The large erosional contrast between the plateau and its flanks is evident from  
362 the variation in erosion rates derived from  $^{10}\text{Be}$  analysis (Fig. 6). The  $^{10}\text{Be}$  analysis  
363 shows that for similar drainage areas, the erosion rates are lower in the Sabana de  
364 Bogotá plateau region (< 20 mm/ka) than on its flanks (>400 mm/ka (Table 3). In more  
365 detail, the upper half of the Guayuriba catchment is eroding at a rate of ~75 mm/ka  
366 (samples LUCN-01, 03, 04, 08; Fig. 6), whereas downstream the erosion rates are  
367 ~100, 479 and 670 mm/ka (LUCN-07, LUCN-05 and LUCN-06). Two samples (LUCN-  
368 05 and LUCN-06) show that erosion rates are an order of magnitude higher than the  
369 rest of the flank samples and provide of the highest erosion rates (see discussion  
370 below). In the Turmequé catchment, the erosion rates increase progressively  
371 downstream from 5.5 mm/ka in the upper part of the catchment in the longitudinal tract  
372 (LUCN-45) to 15.7, 48, 53 and 59 mm/ka (LUCN-26, 28, 27 and 25) in the transverse  
373 tract (Fig.6).

374 The Sogamoso catchment drains the axial plateau of the Eastern Cordillera to the  
375 north, and is eroding at a rate of 167 mm/ka (LUCN-54; Fig. 6). This catchment is  
376 divided into the Suárez catchment in the west and the Chicamocha catchment in the  
377 east, which are eroding at a rate of 64 and 228 mm/ka (LUCN-55 and 56), respectively.  
378 The upper part of the Suárez catchment is eroding at a rate of 8 and 10 mm/ka (LUCN-  
379 46 and 50). The erosion rate for the middle part of the Sogamoso catchment is 46  
380 mm/ka (LUCN-53), and is similar to the erosion rate for the Suárez catchment.

381 TCN exposure ages for terrace boulders in the Guayuriba basin, assuming zero  
382 erosion and considered as minimum ages, range from 257 to 697 ka. However, the  
383 ages will be significantly older if we estimate an erosion rate using the oldest boulder  
384 age (LUCN-12) by applying the methods of Lal (1991). The erosion rate obtained from  
385 the oldest boulder is ~1 mm/ka and if we assume that all the samples erode at this  
386 rate, the initial ages with zero erosion will increase by up 50% for ages up to ~700 ka.



1  
2  
3 387 However, since we sampled large boulders with no apparent weathering, we can  
4  
5 388 assume that a correction factor for erosion is not really necessary for our ages.  
6

7  
8 389 The ranges of ages show significant scatter, but the three oldest samples (LUCN-  
9  
10 390 11 to LUCN-13) clustered particular well given their antiquity, with a mean age of  $656 \pm$   
11  
12 391  $69$  ka. We argue that the two youngest ages probably reflect exhumation of the  
13  
14 392 boulders from the terrace and so we do not use those ages in our incision rate  
15  
16 393 calculation. Given the mean elevation of the three oldest samples is  $2129 \pm 3$  m asl  
17  
18 394 and the elevation in the adjacent valley is  $\sim 1723$  m asl, we use a height difference of  
19  
20 395  $406 \pm 5$  m to calculate an incision rate of  $\sim 62$  mm/ka. This is comparable with the  
21  
22 396 catchment-averaged erosion rates calculated from river sediment from the flank  
23  
24 397 streams.  
25

26  
27 398

## 28 29 399 **5. Discussion**

30  
31  
32 400 Calculated erosion rates for the Eastern Cordillera using  $^{10}\text{Be}$  and values of SSP,  
33  
34 401  $M_x$  and  $\chi$  show clear erosional contrasts between the axial plateau and its flanks. Intra-  
35  
36 402 domain and intra-basin differences are also apparent between regions.  
37

38  
39 403

### 40 41 42 404 *5.1. Drainage network dynamics*

43  
44 405 Rivers across the flanks of the Eastern Cordillera need more erosion capacity  
45  
46 406 than the longitudinal rivers in the Sabana plateau for river capture to occur (Struth et  
47  
48 407 al., 2015). Higher erosion rates along the flanks of the Eastern Cordillera ( $>50$  mm/ka)  
49  
50 408 compared to the Sabana plateau ( $<20$  mm/ka) suggests that retreat of the main divides  
51  
52 409 and capture of the longitudinal plateau rivers by the transverse flank rivers is occurring.  
53  
54 410 The Guayuriba and the Bogotá catchments provide examples of flank catchments with  
55  
56 411 a drainage area of  $200 \text{ km}^2$  yielding an erosion rate of  $79$  mm/ka (LUCN-01), whereas  
57  
58 412 the plateau catchments with comparable drainage areas of  $163$  and  $245 \text{ km}^2$  yield  
59  
60

1  
2  
3 413 erosion rates of 18 (LUCN-30) and 4 mm/ka (LUCN-31), respectively (Fig. 6). For a  
4  
5 414 plateau catchment with an area of 240 km<sup>2</sup>, an erosion rate of 15 mm/ka (LUCN-15)  
6  
7 415 was determined, which is lower than a similar size catchment (293 km<sup>2</sup>) on the eastern  
8  
9 416 flank that has an erosion rate of 77 mm/ka (LUCN-08). Comparisons between the  
10  
11 417 Turmequé and Sogamoso catchments also illustrate this contrast; sampled catchments  
12  
13 418 for Suárez, with areas of 313 and 1186 km<sup>2</sup>, provided rates of 7 and 10 mm/ka (LUCN-  
14  
15 419 46 and 50). This is markedly different from the Turmequé flank samples from drainage  
16  
17 420 areas of 460 and 1291 km<sup>2</sup> that have higher erosion rates of 48 and 59 mm/ka (LUCN-  
18  
19 421 28 and 25), respectively. These results confirm that the main drainage divides in the  
20  
21 422 Eastern Cordillera will migrate towards the axial plateau because rivers in the flanks  
22  
23 423 have more energy (indicted by SSP values) and erosion capacity (reflected in the Mx  
24  
25 424 values).

26  
27  
28 425 A special case is illustrated by comparing the Sabana catchment where sample  
29  
30 426 LUCN-19 was collected (with a drainage area of 265 km<sup>2</sup> and an erosion rate of 11  
31  
32 427 mm/ka) with the Turmequé catchment flank where samples LUCN-45 (65 km<sup>2</sup>, 6  
33  
34 428 mm/ka) and LUCN-26 (346 km<sup>2</sup>, 15 mm/ka) were collected. This sampled area round  
35  
36 429 these samples was interpreted by Struth et al. (2015) as a drainage capture zone on  
37  
38 430 the basis of topography, featuring a depressed topographic profile and a mapped  
39  
40 431 reentrant toward the west of the main divide, and of the occurrence of knickpoints  
41  
42 432 upstream of a fluvial elbow (sharp change in the river channel direction) in map view.  
43  
44 433 Similar erosion rates on both sides of the drainage divide in the Turmequé area argue  
45  
46 434 in favor of drainage capture. In addition, the |<sub>s</sub>-values map shows that the upper part of  
47  
48 435 the Turmequé catchment was part of the plateau area in the past and is now  
49  
50 436 incorporated into the flank domain (Fig. 5B1).

51  
52  
53 437 As documented by Struth et al. (2015), the Eastern Cordillera of Colombia has  
54  
55 438 clear geomorphic differences between its flanks and axial zone, which includes the  
56  
57 439 Sabana de Bogotá and the southern low-relief part of the upper Sogamoso catchment.  
58  
59  
60

1  
2  
3 440 Comparison of the geomorphic indices and the erosion rate results with the drainage  
4  
5 441 divide features argue for capture processes. This confirms the view of Struth et al.  
6  
7 442 (2015) and Babault et al. (2013) who proposed drainage divide migration and a  
8  
9 443 longitudinal to transverse drainage rearrangement in the Eastern Cordillera.

10  
11  
12 444 Correlation of erosion rates with Mx values (Fig. 9) is stronger than with the SSP  
13  
14 445 (Fig. 8). The SSP is, at a first order, a function of precipitation, slope and drainage  
15  
16 446 area. Calculation of the SSP from a series of raster measurements and the low-  
17  
18 447 resolution data of the DEM or the precipitation provide equivocal results. Mx is solely a  
19  
20 448 function of the elevation and distance of the river profile, providing a more realistic  
21  
22 449 value to describe the steepness of the river reaches.

23  
24  
25 450

## 26 27 28 451 *5.2. Calibration of geomorphic parameters*

29  
30 452 The links between erosion rates and SSP or Mx have been examined in previous  
31  
32 453 studies (e.g., Kirby and Whipple, 2012; Perron and Royden, 2013, 2003; Safran et al.,  
33  
34 454 2005; Bookhagen and Strecker, 2012). Our data reveal high erosion rates derived from  
35  
36 455 samples located on the flanks of the Eastern Cordillera (which show high SSP) and in  
37  
38 456 the northern parts of the Sogamoso basin, and low rates for the axial plateau (Sabana  
39  
40 457 de Bogotá, upper part of Turmequé basin and southern part of the Sogamoso basin).

41  
42  
43 458 Geomorphic indices cluster into four groups (A, B, and C in Fig. 8B). Group A  
44  
45 459 comprises Sogamoso catchment samples from the most incised northern part of that  
46  
47 460 catchment (LUCN-53, 54, 55, 56). Group B is associated with flanks that are  
48  
49 461 characterized by high relief, and group C includes the lowest relief area samples.  
50  
51 462 Group C is subdivided into C', including samples with flank characteristics but with  
52  
53 463 lower relief (LUCN-25, 27, 28 and 01), and C'', with plateau characteristics (LUCN-19,  
54  
55 464 26, 31, 33, 45, 46, 50).

1  
2  
3 465 Erosion rates and the catchment-wide average  $Mx$  values correlate positively  
4  
5 466 (Fig. 9). Despite the four samples having different lithologies, climate and uplift  
6  
7 467 conditions (dashed box in Fig. 9), a polynomial equation is defined for the rest of  
8  
9 468 samples (Trend A = red line in Fig. 9). Trend A reflects samples with similar lithologies  
10  
11 469 and in areas of similar precipitation and uplift. This trend is linear and can be expressed  
12  
13 470 in the form:

14  
15  
16 471  $E = a_1 \cdot Mx$  (4)

17  
18  
19 472 where  $a_1$  is 12.28.

20  
21  
22 473 Equation 4 might be used as a proxy for estimating erosion rates when TCN data  
23  
24 474 are not available or cannot be obtained. However, the applicability of equation 4 for the  
25  
26 475 shale-rich western flank of the Eastern Cordillera of Colombia might be problematic.  
27  
28 476 This is because the western flank is a shale-dominated area with more erodible rocks  
29  
30 477 while the eastern flank is composed of alternating of sandstone and shale formations  
31  
32 478 that are more resistant; hence application of equation 4 for the western side will provide  
33  
34 479 underestimates of the erosion rates.

35  
36  
37 480

38  
39 481 *5.3. Local climatic, bedrock and tectonic effects*

40  
41  
42 482 Classifying our samples into 4 groups, according to their erosion rates, provides  
43  
44 483 an additional means of differentiating between the axial plateau and the cordillera  
45  
46 484 flanks (Fig. 10):

47  
48  
49 485 Group I represents the plateau domain, with the lower erosion rate values (<20  
50  
51 486 mm/ka). This area is a relatively little tectonically deformed belt of the cordillera (e.g.,  
52  
53 487 Mora et al., 2008, Teixell et al. 2015), and is associated with longitudinal, structure-  
54  
55 488 controlled fluvial drainage. Samples LUCN-26 and 45 are not located on the plateau,  
56  
57  
58  
59  
60

1  
2  
3 489 but the low relief of these catchments and the longitudinal trend of the rivers suggest  
4  
5 490 they were part of the plateau in the past.  
6  
7

8 491 Group II samples represent an incised domain, including some of the samples  
9  
10 492 located in the flanks and in the Sogamoso catchment (Suárez River). The samples  
11  
12 493 located in this group are from high-energy rivers that are transverse to the chain, and  
13  
14 494 cut across the structural grain.  
15  
16

17 495 Group III includes only two samples, LUCN-54 (167 mm/ka, Sogamoso river) and  
18  
19 496 LUCN-56 (228 mm/ka, Chicamocha river). The difference between erosion rates for  
20  
21 497 these samples and the adjacent catchments, 46 mm/ka (LUCN-53) compared to 64  
22  
23 498 mm/ka (LUCN-55), correlates with a difference in climate, vegetation cover and rock  
24  
25 499 strength. Basement composed of low- and medium-grade metamorphic rocks is  
26  
27 500 exposed in the upper and medium part of the Chicamocha basin (LUCN-56), and the  
28  
29 501 region has little vegetation. In contrast, the Suárez river basin (LUCN-55) mainly  
30  
31 502 traverses alternating Cretaceous sandstone and shale formations. In terms of  
32  
33 503 erodibility, and according to Castro (1992) and González and Jiménez (2015),  
34  
35 504 basement rocks are more erodible than Cretaceous sedimentary rocks. Moreover,  
36  
37 505 erosion is enhanced because of the lack of vegetation cover in the upper and middle  
38  
39 506 part of the Chicamocha basin. The Chicamocha valley has an arid microclimate unlike  
40  
41 507 any other part of the Eastern Cordillera. The valley is very narrow and the obtained  
42  
43 508 data (Fig. 2) from the few pluviometer stations do not reflect the real conditions inside  
44  
45 509 it, resulting in overestimates of precipitation. The Cocuy-Santander massif to the east  
46  
47 510 and the Floresta massif to the west bound the Chicamocha valley (Fig.1). These massifs  
48  
49 511 form an orographic barrier and result in a rain shadow zone within the Chicamocha  
50  
51 512 valley. The Chicamocha river is characterized by a very high mean  $M_x$  (~ 8.13) with  
52  
53 513 steep hillslopes and an erosion rate of  $228 \pm 32$  mm/ka. The Suárez river (sample  
54  
55 514 LUCN-54) mainly flows across Cretaceous formations and  $M_x$  values are low (~ 5.92),  
56  
57 515 with an erosion rate of  $63.8 \pm 8.6$  mm/ka. The Chicamocha catchment, with higher  
58  
59  
60

1  
2  
3 516 erosion rate, has lower precipitation than the Suárez catchment, which is similar to the  
4  
5 517 Sabana de Bogotá. If high precipitation results in large erosion rates, then higher  
6  
7 518 erosion rates would be expected in the wetter Suárez catchment than in the  
8  
9 519 Chicamocha catchment; but this is not the case. We propose that the high erosion rate  
10  
11 520 in the Chicamocha valley is related to the local “semiarid” conditions, low vegetation  
12  
13 521 cover and more erodible bedrock, all of which will enhance the erosion capacity. We  
14  
15 522 underline the importance of rock type in determining the magnitude of the erosion  
16  
17 523 within similar topographic domains, as shown in other studies in dynamic settings  
18  
19 524 where higher denudation rates that have been related to high erodibility of the rocks  
20  
21 525 (e.g., Salgado et al., 2008; Chadwick et al., 2013; Bierman et al., 2014; Pupim et al.,  
22  
23 526 2015). Safran et al. (2005) showed that the rock type might play a secondary non-  
24  
25 527 dominating role in catchment-averaged erosion rates in the Bolivian Andes, where high  
26  
27 528 erosion rates were found in catchments that have weak or resistant bedrock. That work  
28  
29 529 proposed that uplift had first order effect on erosion rates, with rock type playing a  
30  
31 530 second order effect, and climate had little if any influence on erosion. However, rock  
32  
33 531 type, vegetative cover and climate have a first order effect on erosion in the Eastern  
34  
35 532 Cordillera of Colombia.

36  
37  
38  
39 533 Group IV is composed only by two samples, LUCN-05 (479 mm/ka) and LUCN-  
40  
41 534 06 (670 mm/ka), which yielded strongly different erosion rates compared with the rest  
42  
43 535 of the Guayuriba catchment samples, as for example the sample LUCN-03 with an  
44  
45 536 erosion of 73 mm/ka. Group IV samples are located in the Quetame basement massif  
46  
47 537 (that is easily eroded), characterized by higher precipitation values and younger  
48  
49 538 exhumation ages (e.g., Mora et al., 2008, 2010; Parra et al., 2009a) than in the upper  
50  
51 539 part of the catchment, as indicated by greater erosion and incision (see Fig. 2). The  
52  
53 540 combination of greater precipitation and exhumation defines a closed feedback erosive  
54  
55 541 cycle, in accordance with the high erosion rates determined for this area.  
56  
57  
58  
59  
60

1  
2  
3 542 Up to 150 mm/ka differences in erosion rates are observed in catchments within  
4  
5 543 the same topographic domain (Fig. 6). The difference between the Suárez ( $64 \pm 9$   
6  
7 544 mm/ka) and Chicamocha ( $228 \pm 32$  mm/ka) catchments is likely due to a combination  
8  
9 545 of precipitation and lithologic effects. Erosion rates in the eastern flank catchments are  
10  
11 546 not homogeneous, as is, reflected by the Guayuriba basin showing higher erosion  
12  
13 547 rates, relief and incision values than the Turmequé catchment (Figs. 2 and 11).

14  
15  
16 548 The contrast in erosion rates described above argues for different fluvial  
17  
18 549 dynamics between the Guayuriba and Turmequé catchments. The upper part of the  
19  
20 550 Turmequé catchment has clearly been captured, as suggested by geomorphic analysis  
21  
22 551 in Struth et al. (2015). Our current work adds new analysis using the  $\chi$  and SSP values  
23  
24 552 suggesting a rearrangement of the axial longitudinal drainage by transverse rivers that  
25  
26 553 traverse the flanks of the cordillera. The disequilibrium in the  $\chi$  values for both sides of  
27  
28 554 the eastern and central divides suggests drainage divide migration toward the inner  
29  
30 555 part of the plateau's interior and to the north, respectively. This drainage divide  
31  
32 556 migration is more evident for the Turmequé catchment than for the Guayuriba  
33  
34 557 catchment. This supports the view of Struth et al. (2015) who suggested that the  
35  
36 558 Turmequé area was a captured reentrant.

37  
38  
39 559 The different geomorphic characteristics of the eastern drainage divide and  
40  
41 560 between the two catchments are interpreted as the result of the competition between  
42  
43 561 uplift and erosion. In the Guayuriba catchment, the erosive potential results from the  
44  
45 562 high contrast between slopes during mountain building and the active tectonics in the  
46  
47 563 basin that has young thermochronologic ages (Mora et al., 2008, 2010; Parra et al.,  
48  
49 564 2009a; Fig. 2), arguing for high erosive potential to compensate the high uplift in the  
50  
51 565 foothills of the flanks. In this way, the upstream propagation of erosion and then, the  
52  
53 566 capture and divide migration is less probable in a catchment with low exhumation such  
54  
55 567 as the Turmequé catchment.  
56  
57  
58  
59  
60

1  
2  
3 568 Struth et al. (2015) interpret the different river dynamics between the flanks and  
4  
5 569 the axial plateau of the Eastern Cordillera as a product of mountain building and  
6  
7 570 drainage development. As such there was progressive increase in the regional slope  
8  
9 571 caused by the accumulation of crustal shortening and thickening, as documented for  
10  
11 572 the Moroccan High Atlas (Babault et al., 2012). Essentially, the contrast in regional  
12  
13 573 slopes results in different erosion rates and topographic dynamics across the Eastern  
14  
15 574 Cordillera. Variations in local precipitation, tectonics and bedrock within a basin may  
16  
17 575 also influence its erosion dynamics, and may have played a secondary role in the  
18  
19 576 dynamism of divide migration and landscape evolution.  
20  
21  
22 577

## 23 24 25 578 **6. Conclusions**

26  
27 579 A smooth axial plateau flanked by steep topographic belts characterizes the  
28  
29 580 Eastern Cordillera of Colombia. New  $^{10}\text{Be}$  TCN data reveal high erosion rates for  
30  
31 581 catchments along the high-relief flanks of the Eastern Cordillera, with a mean value of  
32  
33 582  $70 \pm 10$  mm/ka (exceeding 400 mm/ka in some catchments). In contrast, the mean  
34  
35 583 erosion rate is of  $11 \pm 1$  mm/ka for the low-relief axial plateau. This argues for erosional  
36  
37 584 contrasts between the two domains and a migration towards the plateau of the N-S  
38  
39 585 oriented plateau-flanks drainage divides. Results of digital morphometric analysis,  
40  
41 586 including specific stream power, steepness index and  $\chi$  values confirm the view that  
42  
43 587 the drainage divide in the Eastern Cordillera is asymmetric and is moving by processes  
44  
45 588 of river capture. Drainage reorganization from longitudinal to transverse, dominated by  
46  
47 589 means of a series of river capture events, will lead to a progressive reduction of the  
48  
49 590 extension of the axial plateau of the Eastern Cordillera. The erosional contrast between  
50  
51 591 the two morphologic domains of the Eastern Cordillera was primarily driven by the  
52  
53 592 increase in the orogen regional slope by progressive accumulation of crustal shortening  
54  
55 593 and thickening. Local climate, tectonics and rock type play a secondary role in  
56  
57 594 controlling the erosion rates and the basin dynamics at a local scale.  
58  
59  
60



1  
2  
3 595 Comparison of the TCN-derived erosion rates with the geomorphic digital  
4  
5 596 parameters show positive correlations with SSP and/or Mx. Using our derived equation  
6  
7 597 (4) the Mx-erosion rate plot for the Eastern Cordillera can be applied to help acquire  
8  
9 598 first-order estimates of erosion rates in areas where there are similar lithologic (layered  
10  
11 599 sedimentary rocks in alternating competent and incompetent formations) and  
12  
13 600 pluviometric characteristics,(but where no TCN data are available  
14  
15 601

### 602 **Acknowledgments**

603 This work was financed by Spanish MINECO projects CGL2010-15416 and  
604 CGL2014-54180-P. L. Struth was supported by a FPI PhD grant (BES-2011-050262)  
605 from MECD (Spain). The stay at the University of Cincinnati for TCN analysis was  
606 supported by MECD grant EEBB-I-14-08485. We acknowledge Sarah Hammer for  
607 laboratory assistance in the University of Cincinnati, and Andrés Mora, Andrés  
608 Valencia, Eliseo Tesón and Maria Luisa Arboleya for assistance and discussion during  
609 fieldwork. We thank the two reviewers of the manuscript for very constructive  
610 comments that significantly improved the original text.

611

### 612 **Supporting Information**

613 Supporting figures: Figure S1, FigureS2

614

### 615 **References**

- 616 Akaike H. 1974. A new look at the statistical model identification. *IEEE Trans. Autom. Control*  
617 **19**: 716–723. DOI:10.1109/TAC.1974.1100705.
- 618 Andriessen PA. M, Helmens KF, Hooghiemstra H, Riezebos PA., Van der Hammen T. 1993.  
619 Absolute chronology of the Pliocene-Quaternary sediment sequence of the Bogota area,  
620 Colombia. *Quaternary Science Reviews* **12** : 483–501. DOI: 10.1016/0277-  
621 3791(93)90066-U
- 622 Babault J, Van Den Driessche J, Teixell A. 2012. Longitudinal to transverse drainage network  
623 evolution in the High Atlas (Morocco): The role of tectonics. *Tectonics* **31** DOI:  
624 10.1029/2011TC003015

1  
2  
3  
4  
5  
6  
7  
8  
9  
10  
11  
12  
13  
14  
15  
16  
17  
18  
19  
20  
21  
22  
23  
24  
25  
26  
27  
28  
29  
30  
31  
32  
33  
34  
35  
36  
37  
38  
39  
40  
41  
42  
43  
44  
45  
46  
47  
48  
49  
50  
51  
52  
53  
54  
55  
56  
57  
58  
59  
60

- 625 Babault J, Teixell A, Struth L, Driessche J Van Den, Arboleya M, Tesón E. 2013. Shortening,  
626 structural relief and drainage evolution in inverted rifts: insights from the Atlas Mountains,  
627 the Eastern Cordillera of Colombia and the Pyrenees. Geological Society of London,  
628 Special Publications **377** : 141–158. DOI: 10.1144/SP377.14
- 629 Bagnold RA. 1966. An Approach to the Sediment Transport Problem from General Physics.  
630 U.S. Geological Survey Geological Survey Professional Paper **422 (1)** : 37.
- 631 Balco G, Stone JO, Lifton N a., Dunai TJ. 2008. A complete and easily accessible means of  
632 calculating surface exposure ages or erosion rates from  $^{10}\text{Be}$  and  $^{26}\text{Al}$  measurements.  
633 Quaternary Geochronology **3** : 174–195. DOI: 10.1016/j.quageo.2007.12.001
- 634 Bayona G, Cortes M, Jaramillo C, Ojeda G, Aristizabal JJ, Reyes-Harker a. 2008. An integrated  
635 analysis of an orogen-sedimentary basin pair: Latest Cretaceous-Cenozoic evolution of  
636 the linked Eastern Cordillera orogen and the Llanos foreland basin of Colombia.  
637 Geological Society of America Bulletin **120** : 1171–1197. DOI: 10.1130/B26187.1
- 638 Van der Beek P, Champel B, Mugnier JL. 2002. Control of detachment dip on drainage  
639 development in regions of active fault-propagation folding. Geology **30** : 471–474. DOI:  
640 10.1130/0091-7613(2002)030<0471:CODDOD>2.0.CO;2
- 641 Bierman PR, Coppersmith R, Hanson K, Neveling J, Portenga EW, Rood DH. 2014. A  
642 cosmogenic view of erosion, relief generation, and the age of faulting in southern Africa.  
643 GSA Today **24** : 4–11. DOI: 10.1130/GSATG206A.1
- 644 Von Blanckenburg F. 2005. The control mechanisms of erosion and weathering at basin scale  
645 from cosmogenic nuclides in river sediment. Earth and Planetary Science Letters **237** :  
646 462–479. DOI: 10.1016/j.epsl.2005.06.030
- 647 Bonnet S. 2009. Shrinking and splitting of drainage basins in orogenic landscapes from the  
648 migration of the main drainage divide. Nature Geoscience **2** : 766–771. DOI:  
649 10.1038/ngeo666
- 650 Bookhagen B, Strecker MR. 2008. Orographic barriers, high-resolution TRMM rainfall, and relief  
651 variations along the eastern Andes. Geophysical Research Letters **35** : 1–6. DOI:  
652 10.1029/2007GL032011
- 653 Bookhagen B, Strecker MR. 2012. Spatiotemporal trends in erosion rates across a pronounced  
654 rainfall gradient: Examples from the southern Central Andes. Earth and Planetary  
655 Science Letters **327-328** : 97–110. DOI: 10.1016/j.epsl.2012.02.005
- 656 Borchers B, Marrero S, Blaco G, Caffee M, Goehring B, Lifton N, Nishiizumi K, Philips F,  
657 Schaefer J, Stone J. 2016. Geological Calibration of spallation production rates in the  
658 CRONUS Earth project. Quaternary Geochronology **31** : 188-198. DOI:  
659 10.1016/j.quageo.2015.01.009
- 660 Bourlès DL. 1988. Etude de la géochimie de l'isotope cosmogénique  $^{10}\text{Be}$  et de son isotope  
661 stable  $^9\text{Be}$  en milieu océanique. Application à la datation des sédiments marins.
- 662 Brown ET, Brook EJ, Raisbeck GM, Yiou F, Kurz MD. 1992. Al in quartz: Implications for  
663 exposure age dating. Geophysical Research Letters **19** : 369. DOI: 10.1029/92GL00266
- 664 Brown ET, Edmond JM, Raisbeck GM, Yiou F, Kurz MD, Brook EJ. 1991. Examination of  
665 surface exposure ages of Antarctic moraines using in situ produced  $^{10}\text{Be}$  and  $^{26}\text{Al}$ .  
666 Geochimica et Cosmochimica Acta **55** : 2269–2283. DOI: 10.1016/0016-7037(91)90103-  
667 C

- 1  
2  
3 668 Burnham KP, Anderson DR. 2002. Model Selection and Multimodel Inference: A Practical  
4 669 Information-Theoretic Approach, 2nd ed., 488 pp., Springer-Verlag, New York, ISBN:0-  
5 670 387-95364-7.
- 6  
7 671 Caballero V, Mora A, Quintero I, Blanco V, Parra M, Rojas LE, Lopez C, Sánchez N, Horton BK,  
8 672 Stockli D, Duddy I. 2013a. Tectonic controls on sedimentation in an intermontane  
9 673 hinterland basin adjacent to inversion structures: the Nuevo Mundo syncline, Middle  
10 674 Magdalena Valley, Colombia. Geological Society, London, Special Publications **377** :  
11 675 315–342. DOI: 10.1144/SP377.12
- 12  
13 676 Caballero V, Parra M, Mora a., Lopez C, Rojas LE, Quintero I. 2013b. Factors controlling  
14 677 selective abandonment and reactivation in thick-skin orogens: a case study in the  
15 678 Magdalena Valley, Colombia. Geological Society, London, Special Publications **377** :  
16 679 343–367. DOI: 10.1144/SP377.4
- 17  
18 680 Castellort S, Goren L, Willett SD, Champagnac J-D, Herman F, Braun J. 2012. River drainage  
19 681 patterns in the New Zealand Alps primarily controlled by plate tectonic strain. Nature  
20 682 Geoscience **5** : 744–748. DOI: 10.1038/ngeo1582
- 21  
22 683 Castro E. 1992. Estado actual de investigación en la cuenca del río Chicamocha,  
23 684 Departamentos de Santander y Boyaca. Ministerio de Minas y Energía. Instituto de  
24 685 investigaciones en geociencias, minería y química. Oficina regional nororiente.
- 25  
26 686 Cerling TE, Craig H. 1994. Geomorphology and In-Situ Cosmogenic Isotopes. Annual Review of  
27 687 Earth and Planetary Sciences **22** : 273–317. DOI: 10.1146/annurev.earth.22.1.273
- 28  
29 688 Chadwick OA, Roering JJ, Heimsath AM, Levick SR, Asner GP, Khomo L. 2013. Shaping post-  
30 689 orogenic landscapes by climate and chemical weathering. Geology **41** : 1171–1174. DOI:  
31 690 10.1130/G34721.1
- 32  
33 691 Colletta B, Hebrard F, Letouzey J, Werner P, Rudkiewicz J-R. 1990. Tectonic style and crustal  
34 692 structure of the Eastern Cordillera (Colombia) from a balanced cross-section. Petroleum  
35 693 and Tectonics in Mobile Belts : 81–100.
- 36  
37 694 Cooper M a, Addison FT, Alvares R, Hayward a B, Howe S, Pulham a J, Taborda a. 1995.  
38 695 Basin development and tectonic history of the Llanos basin, Colombia. Petroleum basins  
39 696 of South America. AAPG. Memoir no. 62 **10** : 659–666
- 40  
41 697 Dortch JM, Owen LA, Haneberg WC, Caffee MW, Dietsch C, Kamp U. 2009. Nature and timing  
42 698 of large landslides in the Himalaya and Transhimalaya of northern India. Quaternary  
43 699 Science Reviews **28** : 1037–1054. DOI: 10.1016/j.quascirev.2008.05.002
- 44  
45 700 Dortch JM, Owen LA, Schoenbohm LM, Caffee MW. 2011. Asymmetrical erosion and  
46 701 morphological development of the central Ladakh Range, northern India. Geomorphology  
47 702 **135** : 167–180. DOI: 10.1016/j.geomorph.2011.08.014
- 48  
49 703 Godard V, Burbank DW, Bours DL, Bookhagen B, Braucher R, Fisher GB. 2012. Impact of  
50 704 glacial erosion on 10Be concentrations in fluvial sediments of the Marsyandi catchment,  
51 705 central Nepal. Journal of Geophysical Research: Earth Surface **117** DOI:  
52 706 10.1029/2011JF002230
- 53  
54 707 Gómez E, Jordan TE, Allmendinger RW, Hegarty K, Kelley S. 2005. Syntectonic Cenozoic  
55 708 sedimentation in the northern middle Magdalena Valley Basin of Colombia and  
56 709 implications for exhumation of the Northern Andes. Bulletin of the Geological Society of  
57 710 America **117** : 547–569. DOI: 10.1130/B25454.1

- 1  
2  
3 711 González JV, Jiménez G. 2015. Análisis estructural y características microtectónicas de un  
4 712 segmento de la falla Bucaramanga en los alrededores del corregimiento Umpalá,  
5 713 Santander. Universidad Industrial de Santander, Bucaramanga.  
6  
7 714 Goren L, Willett SD, Herman F, Braun J. 2014. Coupled numerical-analytical approach to  
8 715 landscape evolution modeling. *Earth Surface Processes and Landforms* **39** : 522–545.  
9 716 DOI: 10.1002/esp.3514  
10  
11 717 Granger DE, Kirchner JW, Finkel R. 1996. Spatially Averaged Long-Term Erosion Rates  
12 718 Measured from in Situ-Produced Cosmogenic Nuclides in Alluvial Sediment. *The Journal*  
13 719 *of Geology* **104** : 249–257. DOI: 10.1086/629823  
14  
15 720 Horton BK, Saylor JE, Nie J, Mora A, Parra M, Reyes-Harker A, Stockli DF. 2010. Linking  
16 721 sedimentation in the northern Andes to basement configuration, Mesozoic extension, and  
17 722 Cenozoic shortening: Evidence from detrital zircon U-Pb ages, Eastern Cordillera,  
18 723 Colombia. *Bulletin of the Geological Society of America* **122** : 1423–1442. DOI:  
19 724 10.1130/B30118.1  
20  
21 725 Howard AD. 1965. Geomorphological systems – equilibrium and dynamics No Title. *American*  
22 726 *Journal of Science* **263** : 302–12.  
23  
24 727 Howard AD, Dietrich WE, Seidl MA. 1994. Modeling fluvial erosion on regional to continental  
25 728 scales. *Journal of Geophysical Research* **99** : 13971–13986. DOI: 10.1029/94JB00744  
26  
27 729 Howard AD, Kerby G. 1983. Channel changes in badlands. *Geological Society of America*  
28 730 *Bulletin* **94** : 739–752.  
29  
30 731 Hurvich C, Tsai C. 1989. Regression and time series model selection in small samples.  
31 732 *Biometrika* **76**: 297–307. DOI: 10.1093/biomet/76.2.297.  
32  
33 733 Jarvis A, Reuter HI, Nelson A, Guevara E. 2008. Hole-filled SRTM for the globe. Version 4.  
34 734 <http://srtm.csi.cgiar.org>  
35  
36 735 Julivert M. 1963. Los rasgos tectónicos de la región de la Sabana de Bogotá y los mecanismos  
37 736 de la formación de las estructuras. *Boletín de Geología Universidad Industrial Santander*  
38 737 **13-14** : 5–102.  
39  
40 738 Julivert M. 1970. Cover and Basement Tectonics in the Cordillera Oriental of Colombia, South  
41 739 America, and a Comparison with Some Other Folded Chains. *Geological Society of*  
42 740 *America Bulletin* **81** : 3623–3646.  
43  
44 741 Kirby E, Whipple K. 2001. Quantifying differential rock-uplift rates via stream profile analysis.  
45 742 *Geology* **6** : 415–418.  
46  
47 743 Kirby E, Whipple KX. 2012. Expression of active tectonics in erosional landscapes. *Journal of*  
48 744 *Structural Geology* **44** : 54–75. DOI: 10.1016/j.jsg.2012.07.009  
49  
50 745 Knighton AD. 1999. Downstream variation in stream power. *Geomorphology* **29**: 293-306.  
51  
52 746 Kohl CP, Nishiizumi K. 1992. Chemical isolation of quartz for measurement of in-situ-produced  
53 747 cosmogenic nuclides. **56** : 3583–3587. DOI: 10.1016/0016-7037(92)90401-4  
54  
55 748 Lal D. 1991. Cosmic ray labeling of erosion surfaces: in situ nuclide production rates and  
56 749 erosion models. *Earth and Planetary Science Letters* **104** : 424–439. DOI: 10.1016/0012-  
57 750 821X(91)90220-C  
58  
59  
60

- 1  
2  
3 751 Lal D, Arnold JR. 1985. Tracing quartz through the environment. Proceedings of the Indian  
4 752 Academy of Sciences - Earth and Planetary Sciences **94** : 1–5. DOI:  
5 753 10.1007/BF02863403  
6  
7 754 Marrero SM, Phillips FM, Borchers B, Lifton N, Aumer R, Balco G. 2016. Cosmogenic nuclide  
8 755 systematic and the CRONUScalc program. Quaternary Geochronology **31** : 160-187.  
9 756 DOI: 10.1016/j.quageo.2015.09.005  
10  
11 757 Mora A, Horton BK, Mesa A, Rubiano J, Ketcham R A, Parra M, Blanco V, Garcia D, Stockli DF.  
12 758 2010. Migration of Cenozoic deformation in the Eastern Cordillera of Colombia  
13 759 interpreted from fission track results and structural relationships: Implications for  
14 760 petroleum systems. AAPG Bulletin **94** : 1543–1580. DOI: 10.1306/01051009111  
15  
16 761 Mora A, Parra M, Strecker MR, Sobel ER, Hooghiemstra H, Torres V, Jaramillo JV. 2008.  
17 762 Climatic forcing of asymmetric orogenic evolution in the Eastern Cordillera of Colombia.  
18 763 Bulletin of the Geological Society of America **120** : 930–949. DOI: 10.1130/B26186.1  
19  
20 764 Moreno CJ, Horton BK, Caballero V, Mora A, Parra M, Sierra J. 2011. Depositional and  
21 765 provenance record of the Paleogene transition from foreland to hinterland basin evolution  
22 766 during Andean orogenesis, northern Middle Magdalena Valley Basin, Colombia. Journal  
23 767 of South American Earth Sciences **32** : 246–263. DOI: 10.1016/j.jsames.2011.03.018  
24  
25 768 Mudd SM, Attal M, Milodowski DT, Grieve SWD, Valters D a. 2014. A statistical framework to  
26 769 quantify spatial variation in channel gradients using the integral method of channel profile  
27 770 analysis. Journal of Geophysical Research: Earth Surface **119** : 138–152. DOI:  
28 771 10.1002/2013JF002981  
29  
30 772 Niemi NA, Oskin M, Burbank DW, Heimsath AM, Gabet EJ. 2005. Effects of bedrock landslides  
31 773 on cosmogenically determined erosion rates. Earth and Planetary Science Letters **237** :  
32 774 480–498. DOI: 10.1016/j.epsl.2005.07.009  
33  
34 775 Nishiizumi K, Imamura M, Caffee MW, Southon JR, Finkel RC, McAninch J. 2007. Absolute  
35 776 calibration of <sup>10</sup>Be AMS standards. Nuclear Instruments and Methods in Physics  
36 777 Research, Section B: Beam Interactions with Materials and Atoms **258** : 403–413. DOI:  
37 778 10.1016/j.nimb.2007.01.297  
38  
39 779 Parra M, Mora A, Jaramillo C, Strecker MR, Sobel ER, Quiroz L, Rueda M, Torres V. 2009.  
40 780 Orogenic wedge advance in the northern Andes: Evidence from the Oligocene-Miocene  
41 781 sedimentary record of the Medina Basin, Eastern Cordillera, Colombia. Bulletin of the  
42 782 Geological Society of America **121** : 780–800. DOI: 10.1130/B26257.1  
43  
44 783 Parra M, Mora A, Jaramillo C, Torres V, Zeilinger G, Strecker MR. 2010. Tectonic controls on  
45 784 Cenozoic foreland basin development in the north-eastern Andes, Colombia. Basin  
46 785 Research **22** : 874–903. DOI: 10.1111/j.1365-2117.2009.00459.x  
47  
48 786 Parra M, Mora A, Sobel ER, Strecker MR, González R. 2009b. Episodic orogenic front migration  
49 787 in the northern Andes: Constraints from low-temperature thermochronology in the  
50 788 Eastern Cordillera, Colombia. Tectonics **28** DOI: 10.1029/2008TC002423  
51  
52 789 Pelletier JD. 2004. Persistent drainage migration in a numerical landscape evolution model.  
53 790 Geophysical Research Letters **31** : L20501. DOI: 10.1029/2004GL020802  
54  
55 791 Perron JT, Richardson PW, Ferrier KL, Lapôtre M. 2012. The root of branching river networks.  
56 792 Nature **492** : 100–3. DOI: 10.1038/nature11672  
57  
58  
59  
60

- 1  
2  
3 793 Perron JT, Royden L. 2013. An integral approach to bedrock river profile analysis. *Earth*  
4 794 *Surface Processes and Landforms* **38** : 570–576. DOI: 10.1002/esp.3302
- 5  
6 795 Pupim N, Bierman PR, Luis M, Rood DH, Silva A, Renato E. 2015. Geomorphology Erosion  
7 796 rates and landscape evolution of the lowlands of the Upper Paraguay river basin ( Brazil )  
8 797 from cosmogenic 10 Be. *Geomorphology* **234** : 151–160. DOI:  
9 798 10.1016/j.geomorph.2015.01.016
- 10  
11 799 Royden L, Taylor Perron J. 2013. Solutions of the stream power equation and application to the  
12 800 evolution of river longitudinal profiles. *Journal of Geophysical Research: Earth Surface*  
13 801 **118** : 497–518. DOI: 10.1002/jgrf.20031
- 14  
15 802 Safran EB, Bierman PR, Aalto R, Dunne T, Whipple KX, Caffee M. 2005. Erosion rates driven  
16 803 by channel network incision in the Bolivian Andes. *Earth Surface Processes and*  
17 804 *Landforms* **30** : 1007–1024. DOI: 10.1002/esp.1259
- 18  
19 805 Salgado AAR, Braucher RV, Colin F, Varajão AFDC, Nalini HA Jr. 2008. Relief evolution of the  
20 806 Quadrilátero Ferrífero (Minas Gerais, Brazil) by means of (10Be) cosmogenic nuclei.  
21 807 *Zeitschrift für Geomorphologie* **52** : 317–323. DOI: 10.1127/0372-8854/2008/0052-0317
- 22  
23 808 Saylor JE, Horton BK, Nie J, Corredor J, Mora A. 2011. Evaluating foreland basin partitioning in  
24 809 the northern Andes using Cenozoic fill of the Floresta basin, Eastern Cordillera,  
25 810 Colombia. *Basin Research* **23** : 377–402. DOI: 10.1111/j.1365-2117.2010.00493.x
- 26  
27 811 Segovia, A., 1965. Mapa Geológico de la plancha L-12 (Medina), de la República de Colombia,  
28 812 Bogotá.
- 29  
30 813 Silva A, Mora A, Caballero V, Rodriguez G, Ruiz C, Moreno N, Parra M, Ramirez-Arias JC,  
31 814 Ibanez M, Quintero I. 2013. Basin compartmentalization and drainage evolution during rift  
32 815 inversion: evidence from the Eastern Cordillera of Colombia. *Geological Society, London,*  
33 816 *Special Publications* **377** : 369–409. DOI: 10.1144/SP377.15
- 34  
35 817 Stone JO. 2000. Air pressure and cosmogenic isotope production. *Journal of Geophysical*  
36 818 *Research* **105** : 23753. DOI: 10.1029/2000JB900181
- 37  
38 819 Struth L, Babault J, Teixell A. 2015. Drainage reorganization during mountain building in the  
39 820 river system of the Eastern Cordillera of the Colombian Andes. *Geomorphology* **250** :  
40 821 370–383. DOI: 10.1016/j.geomorph.2015.09.012
- 41  
42 822 Teixell A, Tesón E, Ruiz JC, Mora A. 2015. The structure of an inverted back-arc rift: insights  
43 823 from a transect across the Eastern Cordillera of Colombia near Bogotá. in C. Bartolini,  
44 824 and P. Mann, eds. *Petroleum Geology and Hydrocarbon Potential of Colombia Caribbean*  
45 825 *Margin: AAPG Memoir*, **108**: 499–516.
- 46  
47 826 Tesón E, Mora A, Silva A, Namson J, Teixell A, Castellanos J, Casallas W, Julivert M, Taylor M,  
48 827 Ibáñez-Mejía M, Valencia VA. 2013. Relationship of Mesozoic graben development,  
49 828 stress, shortening magnitude, and structural style in the Eastern Cordillera of the  
50 829 Colombian Andes. *Geological Society, London, Special Publications* **377** : 257–283. DOI:  
51 830 10.1144/SP377.10
- 52  
53 831 Torres V, Vandenberghe J, Hooghiemstra H. 2005. An environmental reconstruction of the  
54 832 sediment infill of the Bogotá basin (Colombia) during the last 3 million years from abiotic  
55 833 and biotic proxies. *Palaeogeography, Palaeoclimatology, Palaeoecology* **226** : 127–148.  
56 834 DOI: 10.1016/j.palaeo.2005.05.005
- 57  
58  
59  
60

- 1  
2  
3 835 Ulloa C, Rodríguez E. 1979. Geología del Cuadrángulo K12, Guateque. Bol. Geol. Ingeominas  
4 836 **22** : 3–55.  
5  
6 837 Ulloa C, Rodríguez GI. 1982. Intrusiones ácidas ordovícicas y post-devónicas en Floresta  
7 838 (Boyacá). Resum IV Congr. Colombiano Geol. Cali  
8  
9 839 Viaplana M, Babault J, Dominguez S, Van Den Driessche J, Legrand X. 2015. Drainage  
10 840 network evolution and patterns of sedimentation in an experimental wedge.  
11 841 Tectonophysics **664**: 109-124. DOI: 10.1016/j.tecto.2015.09.007  
12  
13 842 Whipple KX. 2001. Fluvial landscape response time: How plausible is steady-state denudation?  
14 843 American Journal of Science **301** : 313–325. DOI: 10.2475/ajs.301.4-5.313  
15  
16 844 Whipple KX, Tucker GE. 1999. Dynamics of the stream-power river incision model: Implications  
17 845 for height limits of mountain ranges, landscape response timescales, and research  
18 846 needs. Journal of Geophysical Research **104** : 17661–17674. DOI:  
19 847 10.1029/1999JB900120  
20  
21 848 Willett SD, McCoy SW, Perron JT, Goren L, Chen C-Y. 2014. Dynamic reorganization of river  
22 849 basins. Science (New York, N.Y.) **343** : DOI: 10.1126/science.1248765  
23  
24 850 Willett SD, Slingerland R, Hovius N. 2001. Uplift, shortening, and steady state topography in  
25 851 active mountain belts. American Journal of Science **301** : 455–485. DOI:  
26 852 10.2475/ajs.301.45.455  
27  
28 853 Yang R, Willett SD, Goren L. 2015. In situ low-relief landscape formation as a result of river  
29 854 network disruption. Nature **520**: 526–529. DOI:10.1038/nature14354.  
30  
31  
32  
33  
34  
35  
36  
37  
38  
39  
40  
41  
42  
43  
44  
45  
46  
47  
48  
49  
50  
51  
52  
53  
54  
55  
56  
57  
58  
59  
60

Sample Number	Qz wt (g)	Be carrier weight (g)	Latitude (°N)	Longitude (°W)	Altitude (m)	$^{10}\text{Be}/^9\text{Be}$ ( $10^{-15}$ )	# of Be-10 atoms ( $10^3$ at/g)
LUCN-01	30.4250	0.3504	4.6201	73.8926	2011	205.91±83.26	162.11±6.55
LUCN-03	23.7496	0.3506	4.5006	73.9040	1565	151.52±9.19	152.90 ±9.27
LUCN-04	30.7997	0.3516	4.4491	73.9048	1466	192.99±9.29	150.61±6.47
LUCN-05	29.6340	0.3514	4.1795	73.7116	719	28.07±4.20	22.76±3.40
LUCN-06	28.7791	0.3502	4.2077	73.8151	928	23.22±2.35	19.31±1.96
LUCN-07	30.3416	0.3504	4.2916	73.8455	1237	127.45±8.80	100.61±6.95
LUCN-08	30.0654	0.3510	4.4008	73.9100	1413	165.88±6.76	132.38±5.39
LUCN-15	30.3979	0.3496	4.4830	74.1217	2686	1225.00±19.35	963.09±15.21
LUCN-19	30.7441	0.3556	5.1087	73.7042	2631	1295.97±27.81	1024.71±21.99
LUCN-25	30.5609	0.3499	5.0873	73.3811	1349	213.23±6.60	166.88±5.16
LUCN-26	30.0070	0.3498	5.2879	73.4013	1953	852.14±15.19	679.07±12.11
LUCN-27	24.3370	0.3504	5.2237	73.3964	1797	200.61±5.61	197.45±5.52
LUCN-28	14.6113	0.3512	5.3216	73.3897	2020	135.99±4.53	223.44±7.44
LUCN-30	30.6254	0.3549	4.7742	73.9559	2516	855.50±22.39	677.71±17.73
LUCN-31	30.1409	0.3496	4.8982	73.8769	2607	3850.15±49.01	3052.79±38.86
LUCN-33	30.4318	0.3520	4.9595	74.0777	2621	1958.19±52.60	1548.36±41.59
LUCN-45	30.8061	0.3500	5.4666	73.4464	2762	3068.09±85.63	2382.89±66.50
LUCN-46	17.5983	0.3510	5.6125	73.6243	2113	944.56±20.83	1287.87±28.40
LUCN-50	21.3327	0.3498	5.9204	73.5932	1641	875.76±17.04	981.67±19.10
LUCN-53	29.7526	0.3502	6.5387	73.1259	1108	226.44±5.57	182.20±4.48
LUCN-54	21.8547	0.3506	6.9023	73.1873	354	52.17±6.16	57.21±6.76
LUCN-55	30.3494	0.3496	6.6232	73.2669	506	164.48±4.95	129.52±3.90
LUCN-56	29.8878	0.3495	6.8246	73.0055	555	63.06±2.66	50.41±2.12

855 **Table 1.**  $^{10}\text{Be}$  sample details for rivers of the Eastern Cordillera including location, Be carrier weight and  $^{10}\text{Be}$  concentrations measured. Carrier  
856 concentration was 1.023 ppm. See sample location in the map of Fig. 3.



Sample	Quartz mass (g)	<sup>9</sup> Be carrier weight (g)	Latitude (°N)	Longitude (°W)	Altitude (m asl)	height/width /breadth clast (cm)	Thickn ess (cm)	Shielding	<sup>10</sup> Be/ <sup>9</sup> Be (10 <sup>-15</sup> )	# of Be-10 atoms (10 <sup>3</sup> )	Exposure age (ka)	External uncertainty (ka)	Internal uncertainty (ka)
LUCN-09	29.765	0.3494	4.4659	73.9325	2133	30/60/80	2	1	3866.38±90.64	310.52±7.27	278	27	7
LUCN-10	30.936	0.3503	4.4672	73.9329	2135	40/40/60	4	1	3686.99±69.19	285.39±5.35	257	24	5
LUCN-11	28.108	0.3519	4.4675	73.9323	2131	40/180/150	3	1	7356.65±116.02	627.81±9.93	614	63	11
LUCN-12	29.743	0.3512	4.4675	73.9322	2129	40/200/400	2.5	1	8644.81±146.22	697.80±11.80	694	73	14
LUCN-13	28.115	0.3516	4.4675	73.9317	2125	50/150/120	3	1	7770.53±134.31	664.29±11.48	659	69	14

857

858 **Table 2.** Description and <sup>10</sup>Be ages for the quartzite boulders on a river terrace in the Guayuriba valley with a carrier concentration of 1023 ppm.

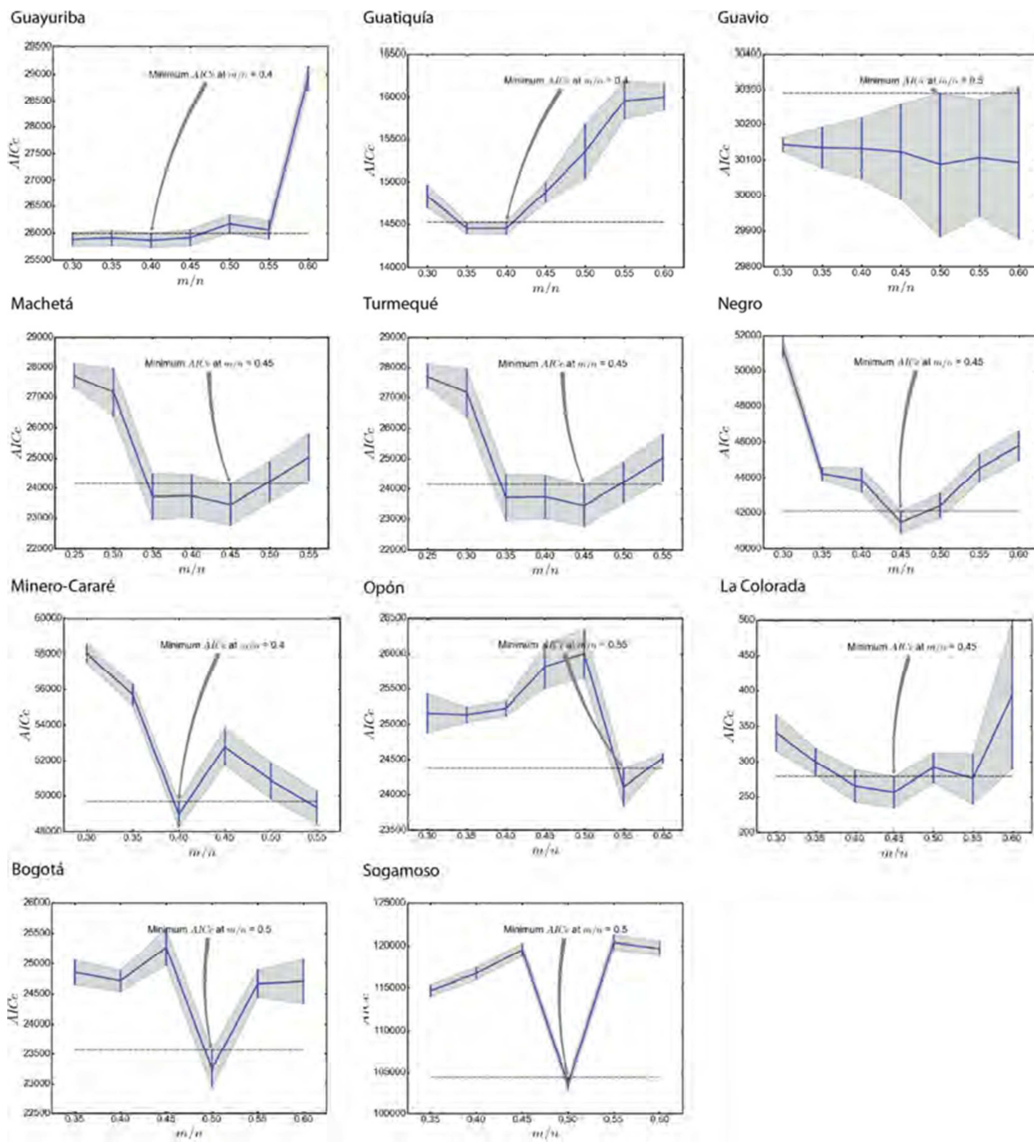
859 See sample location in the map of Figure 3C.

860

Sample	Sample catchment area (km <sup>2</sup> )	Avg. elevation (m)	Standard deviation (m)	MATLAB <sup>10</sup> Be P-rate	<sup>10</sup> Be concentration (10 <sup>5</sup> at/g)	Attenuation length (m)	Erosion rate (mm/ka)	Rainfall rate (mm/a)	SSP (GJ/m2/a)	Mx
LUCN-01	200.5	3071	397	21.3 ± 2.8	1.621 ± 0.065	0.6	79.2 ± 10.9	1331 ± 112	39.28 ± 5.08	7.87 ± 2.77
LUCN-03	526.3	2808	512	18.6 ± 2.4	1.529 ± 0.092	0.6	73.3 ± 10.6	1337 ± 177	51.59 ± 14.28	8.18 ± 2.18
LUCN-04	658.8	2760	531	18.2 ± 2.4	1.506 ± 0.064	0.6	72.6 ± 10.1	1318 ± 186	53.56 ± 16.34	8.43 ± 2.45
LUCN-05	2559.7	2726	701	18.1 ± 2.4	0.227 ± 0.034	0.6	479.4 ± 95.8	1678 ± 684	99.71 ± 63.88	9.28 ± 2.93
LUCN-06	1010.1	3054	685	21.5 ± 2.8	0.193 ± 0.019	0.6	670.7 ± 111.9	1648 ± 453	106.27 ± 53.89	9.81 ± 3.33
LUCN-07	1334.5	2610	560	16.7 ± 2.2	1.006 ± 0.069	0.6	100.1 ± 14.9	1445 ± 327	71.90 ± 35.86	8.64 ± 2.61
LUCN-08	293.1	2645	526	17.0 ± 2.2	1.323 ± 0.053	0.6	77.5 ± 10.7	1280 ± 192	57.60 ± 20.30	9.72 ± 2.51
LUCN-15	239.9	3352	278	24.7 ± 3.2	9.630 ± 0.152	0.6	15.4 ± 2.0	1202 ± 149	33.33 ± 2.16	5.08 ± 1.57
LUCN-19	265.3	2910	189	19.4 ± 2.5	10.247 ± 0.219	0.6	11.4 ± 1.5	923 ± 151	17.62 ± 3.77	2.44 ± 1.46
LUCN-25	1291.2	2605	394	16.5 ± 2.1	1.668 ± 0.051	0.6	59.5 ± 8.0	1094 ± 207	39.53 ± 18.37	5.32 ± 2.37
LUCN-26	345.6	2742	286	17.7 ± 2.3	6.790 ± 0.121	0.6	15.7 ± 2.0	982 ± 81	30.12 ± 8.77	3.73 ± 1.42
LUCN-27	977.2	2708	325	17.4 ± 2.3	1.974 ± 0.055	0.6	53.1 ± 7.1	1008 ± 98	31.78 ± 11.81	4.66 ± 1.85
LUCN-28	459.9	2749	325	17.9 ± 2.3	2.234 ± 0.074	0.6	48.1 ± 6.5	997 ± 98	25.94 ± 5.48	4.82 ± 1.59
LUCN-30	162.5	3010	200	20.5 ± 2.7	6.777 ± 0.177	0.6	18.2 ± 2.4	1045 ± 110	21.58 ± 6.12	6.48 ± 1.1
LUCN-31	244.6	2961	264	20.0 ± 2.6	30.527 ± 0.388	0.6	3.9 ± 0.5	1152 ± 180	19.26 ± 5.72	3.35 ± 1.43
LUCN-33	134.9	3072	250	21.2 ± 2.8	15.483 ± 0.415	0.6	8.3 ± 1.1	1054 ± 125	19.54 ± 2.98	3.12 ± 1.83
LUCN-45	64.9	3119	174	21.8 ± 2.8	23.828 ± 0.665	0.6	5.5 ± 0.7	1097 ± 133	20.52 ± 0.57	2.8 ± 0.57
LUCN-46	313.4	2592	305	16.3 ± 2.1	12.878 ± 0.284	0.6	7.6 ± 1.0	1072 ± 90	17.46 ± 3.02	1.89 ± 1.28
LUCN-50	1185.8	2545	401	16.0 ± 2.1	9.816 ± 0.191	0.6	9.8 ± 1.3	1221.61 ± 268.18	34.50 ± 22.07	3.58 ± 3.07
LUCN-53	2083.3	2251	738	14.0 ± 1.8	1.822 ± 0.044	0.6	46.4 ± 6.2	2101.65 ± 577.49	80.70 ± 29.59	5.72 ± 2.12
LUCN-54	20153.1	2441	777	15.9 ± 2.1	0.572 ± 0.067	0.6	167.1 ± 29.6	1618.68 ± 630.75	95.79 ± 91.41	7.01 ± 4.78
LUCN-55	9789.2	2232	650	13.7 ± 1.8	1.295 ± 0.039	0.6	63.8 ± 8.6	1889.11 ± 716.5	78.81 ± 60.33	5.92 ± 4.78
LUCN-56	9307.1	2792	720	19.1 ± 2.5	0.504 ± 0.021	0.6	228.4 ± 31.7	1360.68 ± 399.12	86.02 ± 59.49	8.13 ± 4.72

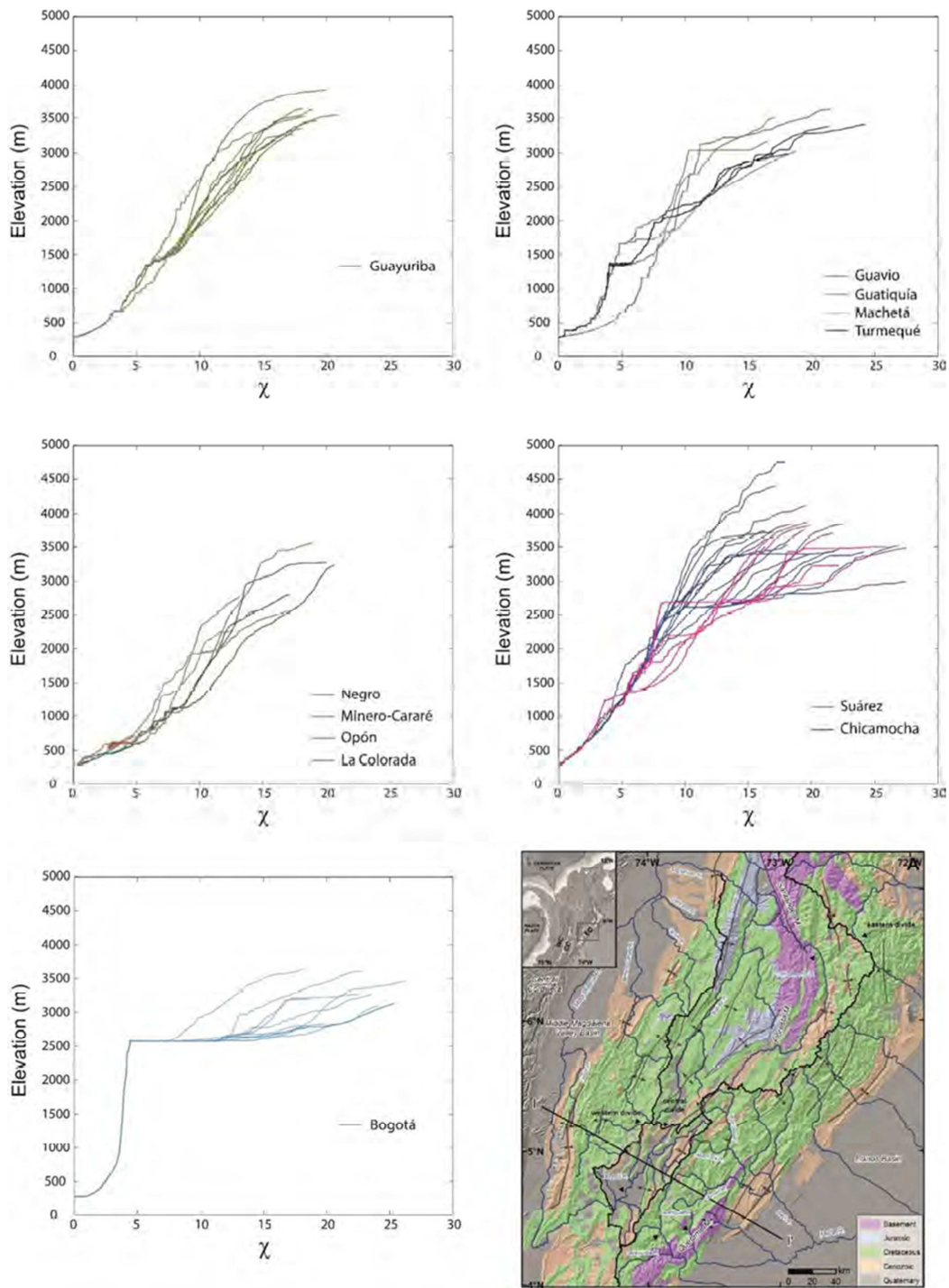
861 **Table 3.** <sup>10</sup>Be TCN data for samples of the Eastern Cordillera. Also shown are rainfall, SSP and Mx values for each sampled basin.

SupplementaryData

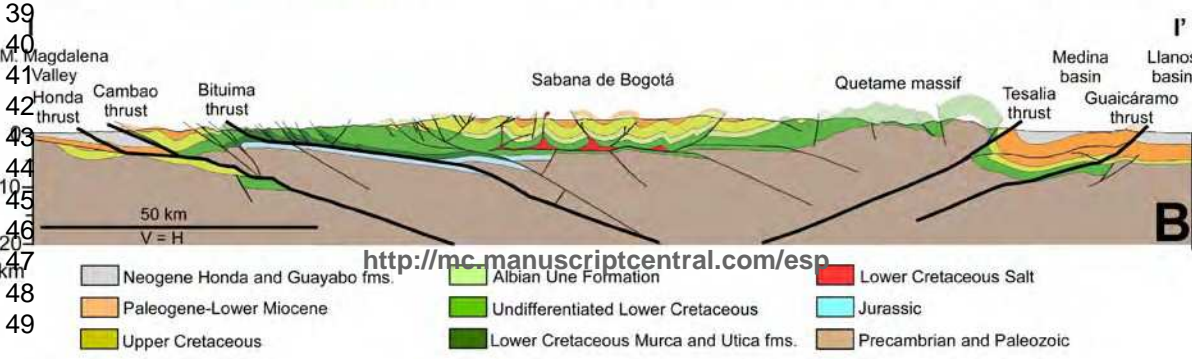
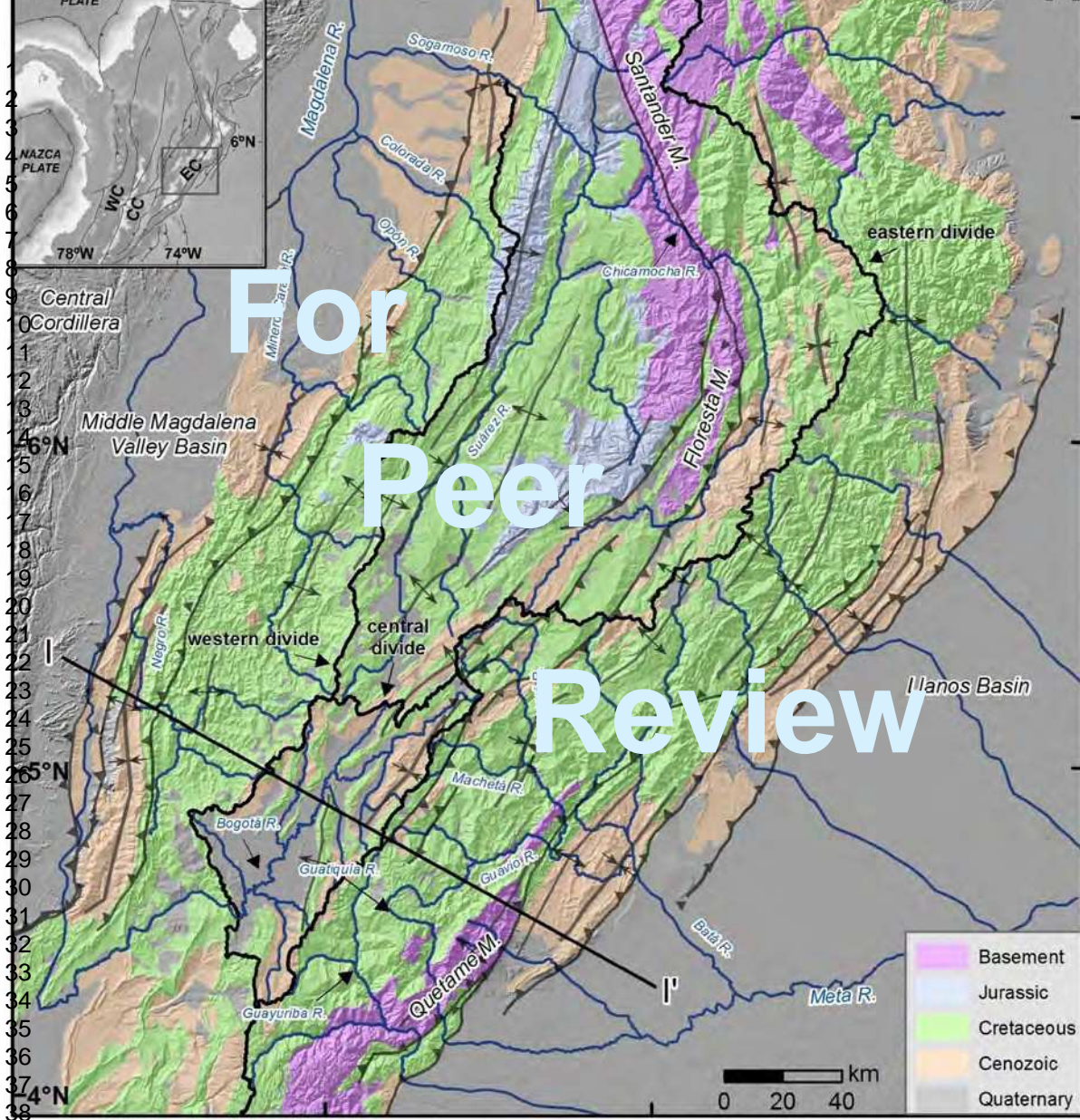


**SD1:** AICc versus m/n plots for the studied basins. The main value is 0.45

1  
2  
3  
4  
5  
6  
7  
8  
9  
10  
11  
12  
13  
14  
15  
16  
17  
18  
19  
20  
21  
22  
23  
24  
25  
26  
27  
28  
29  
30  
31  
32  
33  
34  
35  
36  
37  
38  
39  
40  
41  
42  
43  
44  
45  
46  
47  
48  
49  
50  
51  
52  
53  
54  
55  
56  
57  
58  
59  
60



**SD2:** Chi plots for  $m/n$  ratio of 0.45 and the Figure 1 of the main text for location reference.



39  
40  
41  
42  
43  
44  
45  
46  
47  
48  
49

<http://mc.manuscriptcentral.com/esp>

7°N

2

3

4

5

6

7

8

9

10

11

12

13

14

15

16

17

18

19

20

21

22

23

24

25

26

27

28

29

30

31

32

33

34

35

36

37

38

39

40

Middle Magdalena Valley Basin

For  
Peer  
Review

Charalá

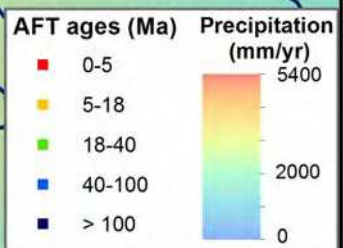
Llanos Basin

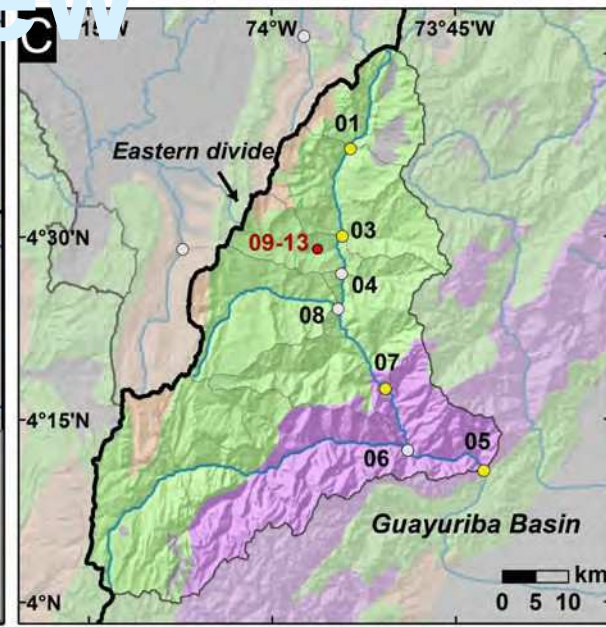
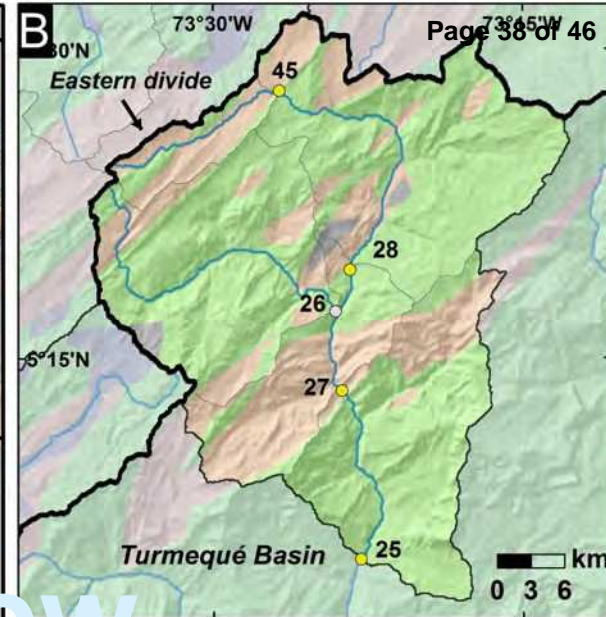
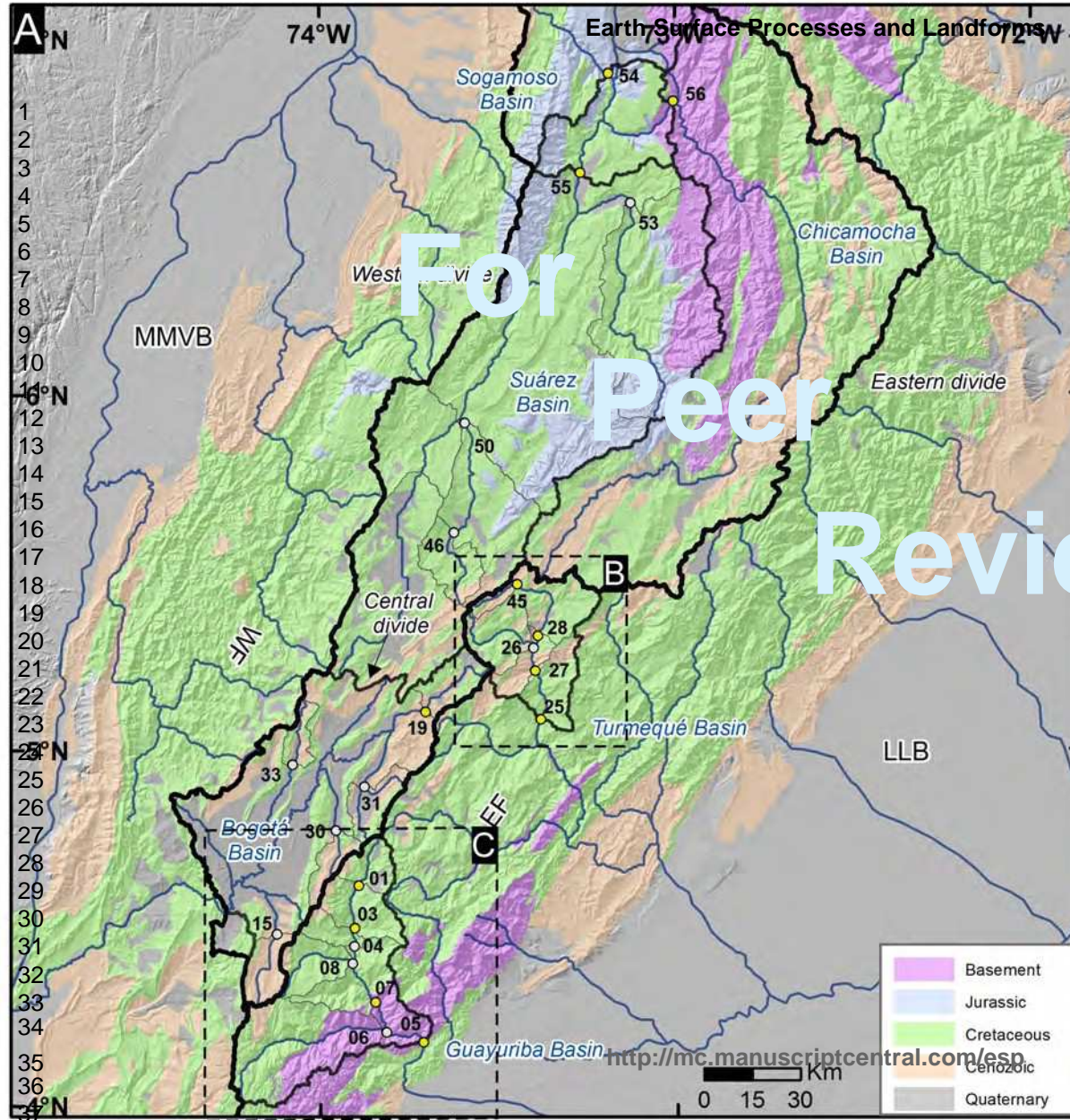
Sabana de Bogotá

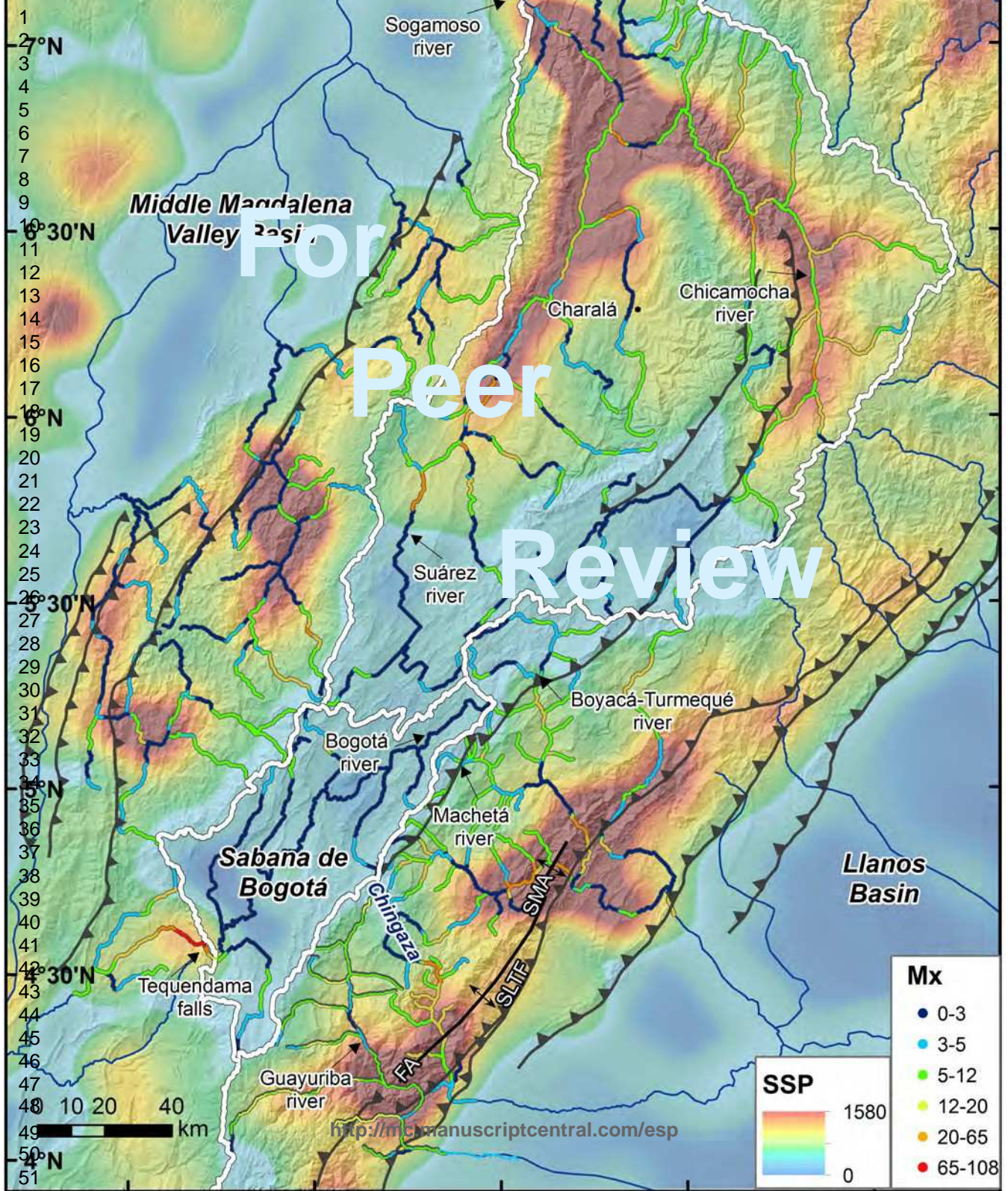
QM

<http://mc.manuscriptcentral.com/esp>

0 10 20 40 Km







Middle Magdalena Valley Basin

For Peer Review

Sogamoso river

Charalá

Chicamocha river

Suárez river

Boyacá-Turmequé river

Bogotá river

Machetá river

Sabana de Bogotá

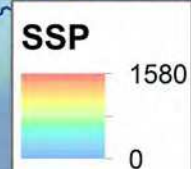
Llanos Basin

Tequendama falls

Guayuriba river

Chingaza

SLTIE SMA

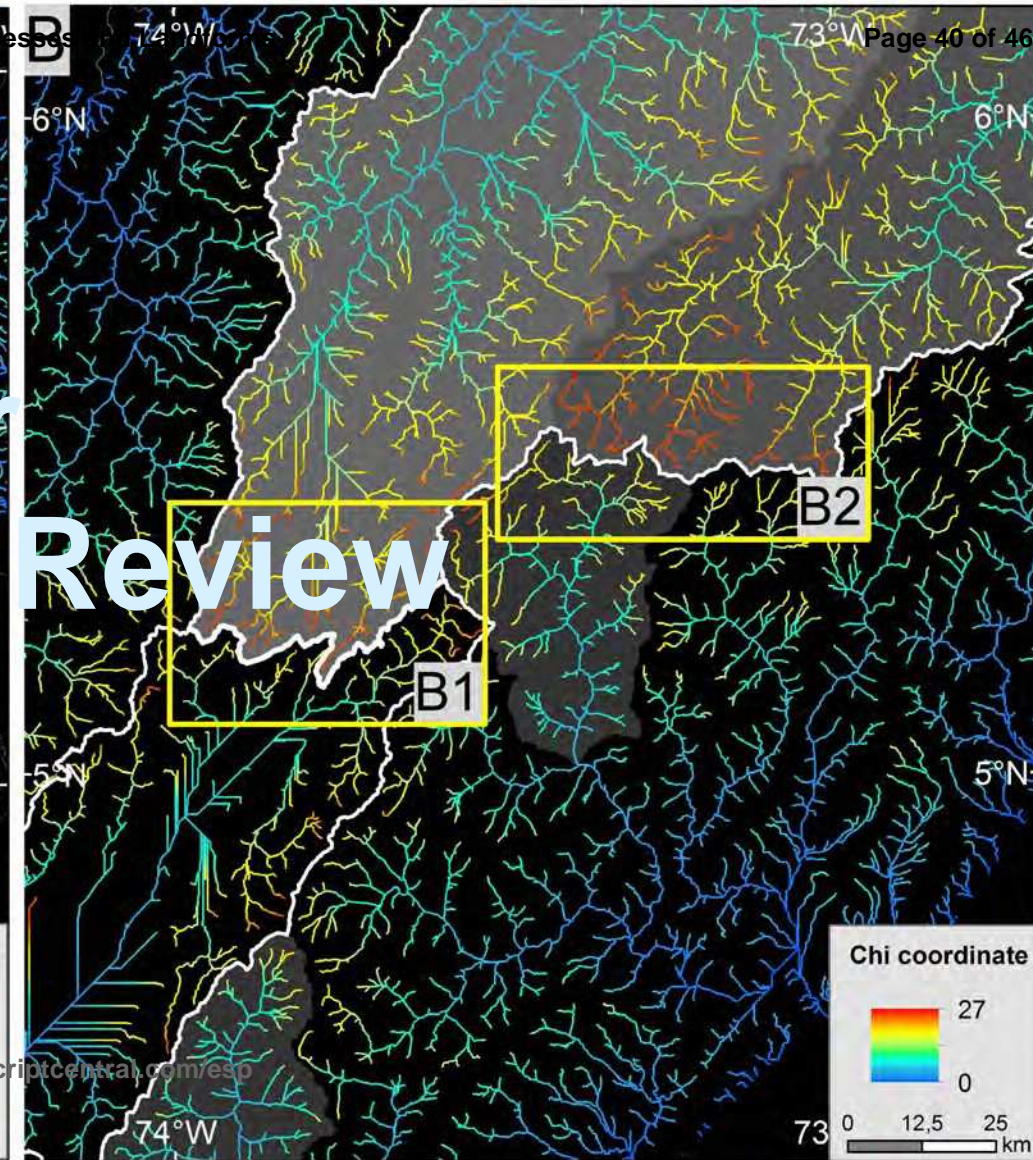
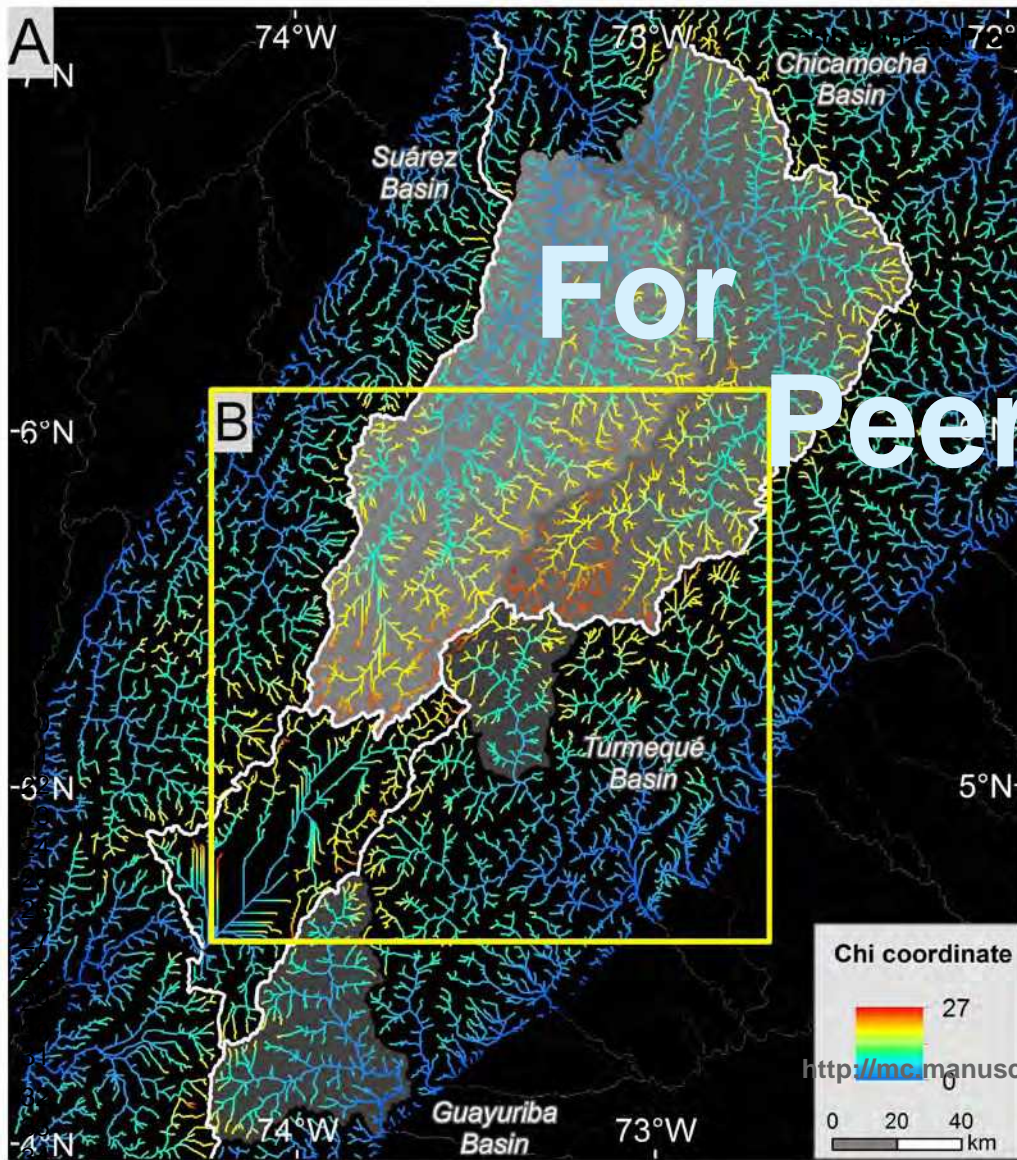


Mx
0-3
3-5
5-12
12-20
20-65
65-108

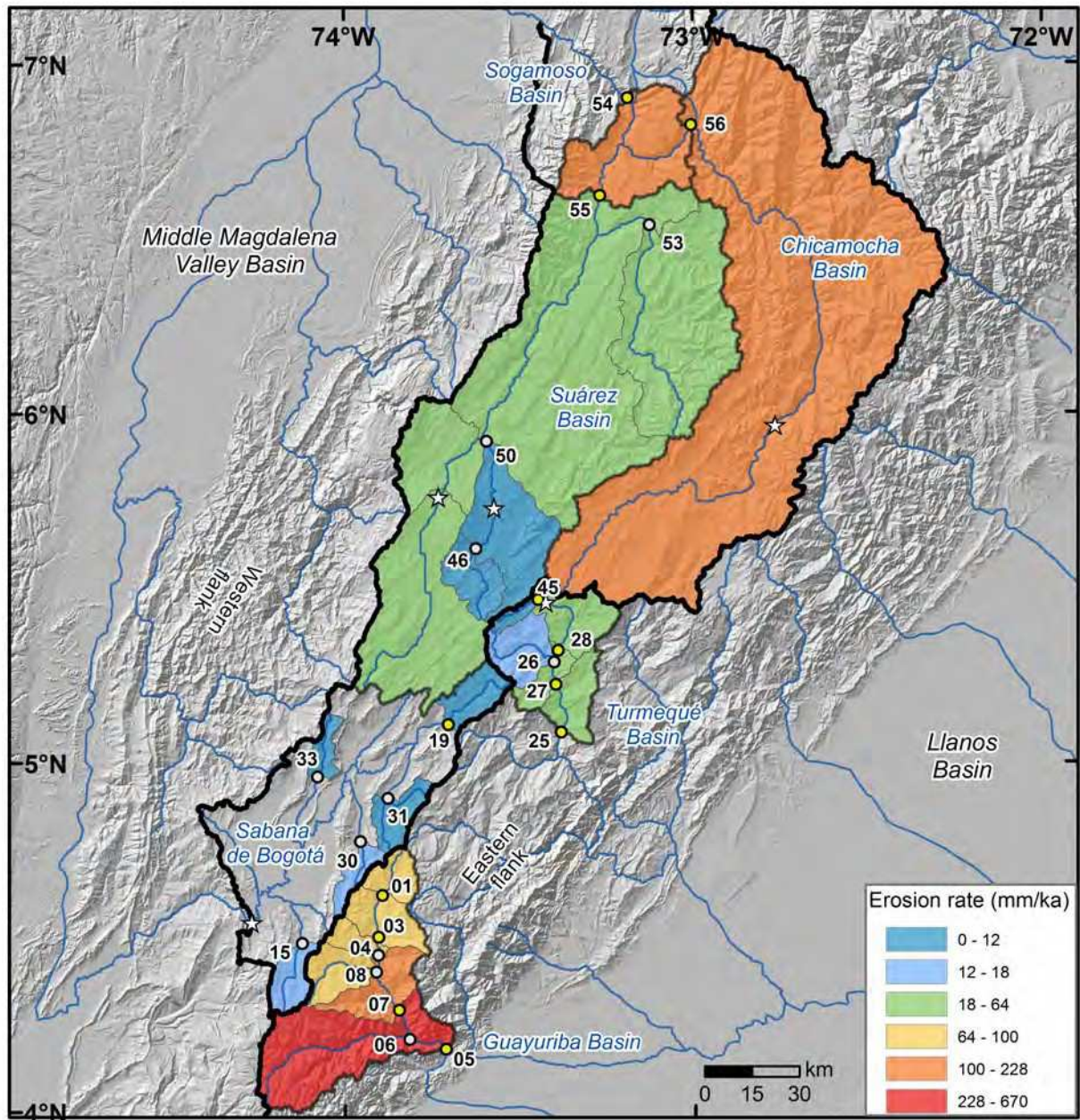


http://mc.manuscriptcentral.com/esp





For Peer Review



ERROR: syntaxerror  
OFFENDING COMMAND: --nostringval--

STACK:

false